MODEL UNCERTAINTY AND TEST OF A SEGMENTED MIRROR TELESCOPE

THESIS

Luke C. Dras, Captain, USAF

AFIT-ENY-14-M-18

DEPARTMENT OF THE AIR FORCE
AIR UNIVERSITY

AIR FORCE INSTITUTE OF TECHNOLOGY

Wright-Patterson Air Force Base, Ohio

AFIT-ENY-14-M-18

MODEL UNCERTAINTY AND TEST OF A SEGMENTED MIRROR TELESCOPE

THESIS

Presented to the Faculty

Department of Aeronautics and Astronautics

Graduate School of Engineering and Management

Air Force Institute of Technology

Air University

Air Education and Training Command

In Partial Fulfillment of the Requirements for the

Degree of Master of Science in Aeronautical Engineering

Luke C. Dras, BS

Captain, USAF

March 2014

AFIT-ENY-14-M-18

MODEL UNCERTAINTY AND TEST OF A SEGMENTED MIRROR TELESCOPE

Luke C. Dras, BS
Captain, USAF

Approved:

//signed//	03/17/2014
Richard G. Cobb, PhD (Chair)	Date
//signed//	03/17/2014
Alan L. Jennings, PhD (Member)	Date
//signed//	03/17/2014
Brandon T. Cesul, PhD (Member)	Date

Abstract

The future of large aperture telescopes relies heavily on the development of segmented array designs. Today's monolithic mirror technology has reached a barrier, particularly for space-based telescopes. These large diameter, dense mirrors allow stable high-resolution imaging but are incompatible with optimized space launch. Segmented mirror telescopes are designed to balance lightweight with compact stowage. The structure necessary to support the flexible mirror array often combines isogrid geometry and complex actuation hardware.

High-fidelity finite element models are commonly used to economically predict how the optics will perform under different environmental conditions. The research detailed herein integrates superelement partitioning and complexity simplifying techniques, resulting in a 92% size reduction of a nodally dense ($>1x10^6$ degrees of freedom) model to allow efficient tuning and validation. Measured vibration data of a segmented mirror telescope was collected to allow system characterization and preliminary tuning. A single frequency comparison tuning iteration decreased the model's error in predicting system dynamics, up to 500 Hz, by 4% on average.

Results demonstrate it is possible to drastically reduce a model size while preserving analytical accuracy. The methodologies presented, applied to similar models with complex isogrid structures, would allow efficient model validation using standard equipped US Air Force desktop computers.

To my father

for teaching and inspiring me to explore the unknown,
live life to the fullest, and believe in the universe's Creator

Acknowledgments

I would like to express my sincere appreciation to my research advisor, Dr. Richard Cobb, for his guidance and insights throughout the course of this thesis effort. I would also like to thank Dr. Alan Jennings who provided valuable background knowledge and support for all facets of my research.

This effort could not have been completed without the commitment of my sponsor, the Naval Postgraduate School, and their dedication to research in the field of optical control systems. Special thanks go to John Bagnasco, Albert Jordan, and Eva Carrillo at the Naval Postgraduate School who provided tireless support for all AFIT modal testing needs and their insight to any issues that arose in modeling the Segmented Mirror Telescope.

Luke C. Dras

Table of Contents

Page

List of Figures

List of Tables

List of Acronyms

AETC: Air Education and Training Command
AFIT: Air Force Institute of Technology
AFOTEC: Air Force Operational Test & Evaluation Center
AFRL: Air Force Research Lab
AIAA: American Institute of Aeronautics and Astronautics
CCA: course control actuator
DLR: diffraction limited resolution
dof: degrees of freedom
DOT: Deployable Optical Telescope project
EOM: equation of motion
FCA: fine control actuator
FCD: Face-Centered Cubic Design
FEA: finite element analysis
FEM: finite element model
FRF: frequency response function
FSA: face sheet actuator
HiFi-FEM: high-fidelity finite element model
ISR: intelligence, surveillance, and reconnaissance
JWST: James Webb Space Telescope
NPS: Naval Postgraduate School
PMA: proof mass actuator
rms: root mean square
RO-FEM: reduced-order finite element model
ROSE-FEM: reduced-order superelement finite element model
SE-FEM: superelement finite element model
SEID: superelement identifier
SMT: Segmented Mirror Telescope
SNR: signal-to-noise ratio
SUITE: Satellite Ultraquiet Isolation Technology Experiment
TMD: tuned mass damper
VISS: Vibration Isolation, Suppression, and Steering project

MODEL UNCERTAINTY AND TEST OF A SEGMENTED MIRROR TELESCOPE

I. Introduction

Background

Diffraction limited resolution is defined by the size of the telescope's primary aperture. The largest space-based imaging telescope, with a primary mirror diameter of 3.5 meters, was the European Space Agency's Herschel Space Observatory (non-resolved imaging system for astronomy) which operated from 2009-2013. Large diameter space telescopes serve many different roles from observation of the distant universe to military intelligence, surveillance, and reconnaissance (ISR) applications. However, they have all had a common design: a monolithic primary mirror. A telescope's aperture, equivalent to the diameter of its primary mirror, is the critical factor to determining resolution limits of a telescope. For space telescopes this diameter is restricted by the payload shroud of the launch vehicle. Additionally, mirror weight can potentially exceed the available payload mass budget because monolithic primary mirrors are regularly created from a single glass slab.

An emerging design concept for space applications is the segmented mirror telescope. This concept allows substantially larger primary mirror diameters using current launch systems. Consisting of multiple smaller mirror segments arranged into an array to act as a single primary mirror, a segmented mirror telescope can be stowed compactly for launch, illustrated in Figure 1, and deployed once on orbit. In addition, the

individual segments can be constructed with lighter materials, ultimately allowing larger apertures at a fraction of a typical monolithic mirror weight.

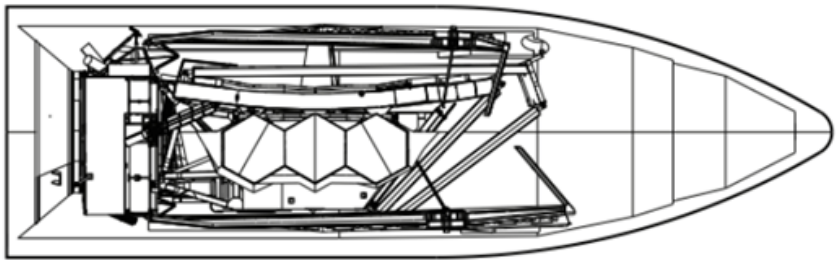

Figure 1. James Webb Space Telescope stowed illustration (NASA, 2014)

As with any optical imaging application, vibrations will distort and degrade image resolution. Segmented mirrors for space application are particularly susceptible as the lightweight segments can have substantial flexibility across the full diameter of the mirror. Therefore, the segments must be precisely controlled through a complex interaction of supporting structure, joints, and actuators. Various vibration sources such as onboard mechanical devices or environmental disturbances contribute to what is referred to as image jitter. The understanding of a space telescope's dynamic response to vibration sources is vital as it allows the design and implementation of a jitter control system.

Problem Statement

Because space telescopes represent a unique and complex engineering challenge, it is common to rely heavily on modeling and simulation techniques in the development of the system. Finite element modeling provides the capability to accurately predict a system's response to disturbances. However, these models are often extremely complex, requiring considerable computing resources for tuning, validating, and analyzing a structural model. It is common to find finite element models (FEM) are created directly

from a manufacturing (dimensional and material property based) model. This method ensures a high-fidelity FEM with regard to geometry, which is often sufficient for analysis of static loading schemes but will often be inefficient for modal analysis. In addition, modeling challenges such as joints and interfaces between materials can lead to inaccuracies in Finite Element Analysis (FEA).

Research Focus

The Segmented Mirror Telescope (SMT), originally developed for the National Reconnaissance Office and since given to the Naval Postgraduate School (NPS) Spacecraft Research and Design Center, is a laboratory deployable, lightweight optical telescope. The telescope serves as an experimental testbed used to demonstrate adaptive optics and other imaging telescope technologies. Though it contains state of the art technology and lightweight construction, the telescope was only intended as a research and development system. The SMT is housed in a dark tent to isolate the telescope from stray light, air currents, or dust and other debris. However, the closed volume is prone to internal acoustic waves. The enclosure is created from thin metal panels and supported by a steel truss structure. With its length of 16 m, the first three acoustic modes of the enclosure are at 11, 21 and 32 Hz (Yingling, 2012, pp. 147-148). The telescope is mounted horizontally on a pneumatic isolation table with an extension to allow test equipment to be placed on the table. The isolators are tuned for seismic disturbances of frequencies below 10 Hz (Jennings & Cobb, 2013, p. 2).

The telescope's basic configuration is that of a Cassegrain reflector with a large concave primary mirror and smaller secondary mirror mounted on a tower, as shown in Figure 2. Located behind the primary mirror are additional sensors like a Shack-

Hartmann wavefront sensor and adaptive optics devices such as a fast steering mirror for global tip and tilt motion correction. The primary mirror is composed of six hexagonal segments that each have six coarse control actuators (CCA) for segment phasing control, three fine control actuators (FCA) for segment local tip/tilt and piston control, and 156 face-sheet actuators (FSA) for segment surface control. The six segments combined form a three meter primary mirror aperture, with each segment being one meter wide. Each segment is constructed from a triangular isogrid silicon carbide substrate upon which the FSAs are mounted. A nanolaminate optical layer is applied to the surface of the substrate for light reflection in the desired wavelength. Each segment is joined to a petal support structure through the FCAs and CCAs providing control in all six degrees of freedom (dof).

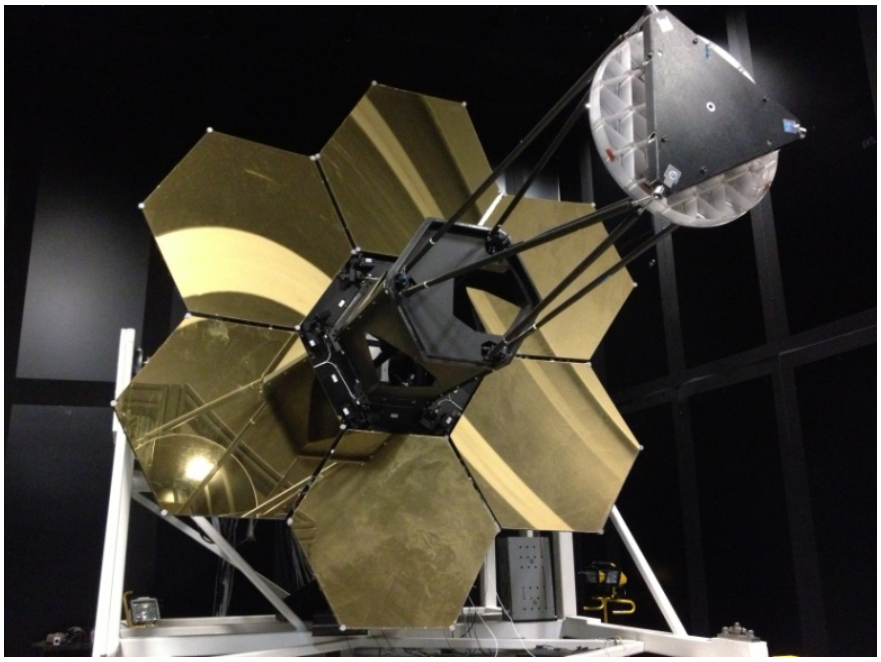

Figure 2. SMT three meter Cassegrain reflector with six segment primary mirror

A high-fidelity FEM of the SMT, with approximately 3.26 million dof, was previously developed to include all optics and associated structure and sensors. The

nodally dense (>1x10^6 dof) model has never been tuned and validated to provide accurate predictions for dynamic response characteristics. Therefore, an efficient reduced-order model that can provide FEA is desired for furthering research in segmented mirror space telescopes.

The primary effort of this research is to accurately characterize the dynamic behavior of a large segmented space telescope based on FEA techniques using a reduced-order model. To achieve this objective, an existing FEM must be decomposed into substructures representing relative physical degrees of freedom of the system. Each substructure is represented with dynamically equivalent but lower dof elements. Using the reduced-order model, experimental test data can be used to adequately tune the FEM. With a tuned FEM, vibration damping and control mechanisms can be designed to attenuate or eliminate problematic characteristics that degrade the optical capability of the telescope.

Methodology

Obtaining a valid FEM requires model tuning analysis iterations. An objective function is developed, then model design variables are varied until analytical results adequately compare to objective function criteria. Most often the objective function is developed as a function of modal characteristics (eigenvalues and eigenvectors) and represents the correlation between simulated predictions and empirical data extracted through experimentation. Analytical solutions must be obtained by incrementally adjusting FEM design variables such as a material's Young's Modulus and/or mass density properties. A high-fidelity FEM (HiFi-FEM) is not desirable as each analysis requires considerable computing resources and time. A reduced-order model that

adequately approximates dynamic characteristics is therefore preferred for performing the iterative model tuning approach.

The process of obtaining a valid FEM of the SMT can be broken down into four fundamental efforts. First, a HiFi-FEM eigenanalysis is conducted to predict system natural frequencies and mode shapes. Second, modal testing of the SMT must be performed to obtain actual natural frequencies, mode shapes, and an estimate of structural damping. Discrepancies between the predicted and actual dynamic characteristics can then be tuned out of the model. Therefore, a reduced-order superelement model (ROSE-FEM) is created to allow timely tuning analysis. Finally, key design variables of the ROSE-FEM are identified and adjusted iteratively to minimize model error.

Assumptions/Limitations

As a pre-developed HiFi-FEM of the SMT was provided in support of this research, several assumptions were made regarding the model. The provided FEM was assumed to be spatially accurate with correct material properties. Nonstructural items, such as wiring harnesses and connectors, are assumed to have insignificant effect on the dynamics of the system and therefore are only modeled as rigid masses. Damping of the mirror segments' modal response, excluding the fundamental frequencies dampened by installed tuned mass dampers, is considered negligible. In addition, the SMT is mounted by six isolation rods to a base structure affixed to an isolation table. Modeled boundary conditions assume the isolation rods are solidly fixed to the base structure.

From previous work by Jennings and Cobb (Jennings & Cobb, 2013), low frequency global modes of the SMT were experimentally determined but limited data was collected on modes greater than 100 Hz. In this work, modal testing concentrated on

high frequency modes (150 to 500 Hz) for three of the six segments. Vibration measurements are assumed accurate as well-developed modal testing procedures were implemented. Gravitational effect on the frequency response measurements was previously found to be negligible (Jennings & Cobb, 2013, p. 13) and therefore not included in the FEA.

Implications

With a tuned FEM, an accurate line-of-sight model can be generated allowing the computation of mirror surface root mean square (rms). With an adaptive optics control scheme, degradation in image resolution due to vibration jitter and wavefront disturbances can be mitigated, minimizing external contributions to the rms figure.

While this research effort focuses solely on modeling and modal testing of the SMT, the methodology can be applied to any ground or space-based segmented mirror system. All applications requiring high-resolution imaging using lightweight structures (with low frequency modes) must consider possible effects from disturbances causing jitter.

Preview

Further background on segmented mirror telescope technology and key modeling techniques researched is provided in Chapter II. The specific methodology implemented to develop a reduced-order FEM of the SMT, along with the experimental data collection procedure, is detailed in Chapter III. A comparison between the original HiFi-FEM and the reduced-order superelement FEM (ROSE-FEM) and modal testing results are provided in Chapter IV. Chapter V presents overall research conclusions and suggestions for future work.

II. Space-Based Segmented Mirror Telescopes: Concept to Realization

Impetus for Large-Aperture Telescopes

Humanity has always had an innate desire to expand its boundaries. The development of the telescope has allowed for the exploration of regions beyond physical reach. Improvement to image resolution has been the continual challenge to the optics community. The Rayleigh criterion, a metric for estimating optical system resolution, was formulated in the late 19th century by Lord J. Rayleigh. From this criterion a measure known as diffraction limited resolution (DLR) was developed to quantify the point separation limit for airy disk imaging (circular aperture approximation excludes wavefront disturbance effects). DLR, in terms of the distance between the optic and object of interest *R*, is shown in Equation (1). This equation relates the theoretical optimum resolution with the diameter of aperture *D* and the wavelength of interest λ (Hecht, 2002, p. 224).

$$DLR = 1.22 \frac{\lambda R}{D} \tag{1}$$

The resolution limitation described by this equation has driven the scientific community into building progressively larger-aperture telescopes; the largest ground-based telescope example thus far being the Thirty Meter Telescope expected to be completed within the decade (Caltech, University of California, 2014). With space-based telescopes intended for Earth observation, aperture diameter contributes to the trade space for achieving increasingly better resolution. Object distance and wavelength remain relatively constant. Orbit altitude is set at a distance required to achieve adequate dwell time over a region of interest and wavelength is set based upon the system's mission.

Recent Work with Segmented Mirror Telescopes

A 2010 white paper produced by the RAND Corporation and NASA Marshall summarizes current space mirror technology, future possibilities, and primary challenges. Due to the need for large-aperture primary mirrors, system production and deployment have been identified as "the most significant technical challenge for future space telescopes" and that "for very large apertures, segmented geometries are the only path forward (Baiocchi & Stahl, 2010, p. 1)." NASA, in cooperation with the European and Canadian space agencies, has been developing the 6.5 meter, 18 segment, James Webb Space Telescope (JWST) since 1996, with a planned launch no earlier than 2017. To advance segmented mirror technology, the NPS established a SMT laboratory to support adaptive optics research, a critical tool for the success of a space-based segmented mirror telescopes.

Vibration Damping and Control for Segmented Mirror Telescopes

The industry minimum for high-resolution mirrors requires the cumulative effect of all surface irregularities be less than $\lambda/4$ (≈158 nm rms in the visible spectrum) (Schwartz, 2013). With state-of-the-art large aperture telescopes, surface figure errors in mirror fabrication commonly range from 8-20 nm leaving an error budget of no more than 150 rms to account for external perturbation sources such as structural vibrations and thermal warping. In addition, increased scaling to the mirror diameter exponentially decreases mirror stiffness independent of the material utilized for the mirror substrate, often being glass, beryllium, or silicon carbide (Baiocchi & Stahl, 2010, p. 6). Space platforms are commonly subjected to various disturbances such as onboard attitude control systems (gyros, reaction wheels, attitude thrusters, etc.) and mission specific

systems (beam steering mirrors, rotating solar panels, etc) (O'Keefe, 2011, p. 157). Segmented mirrors, with inherently low stiffness in comparison to monolithic mirrors, are extremely susceptible to performance degradation due to vibrations. Adaptive optics provide a solution to attenuate vibration amplitudes without adding substantial weight or supporting structure to the system. The Air Force Research Lab (AFRL) has investigated methods to mitigate vibration perturbations. The 1998 Vibration Isolation, Suppression, and Steering (VISS) project and 2003 Satellite Ultraquiet Isolation Technology Experiment (SUITE), implementing vibration suppression through both active and passive isolation techniques, separated sensitive systems from disturbance sources with a six degree of freedom hexapod Stewart platform (Cobb & Sullivan, 1999, p. 804). Additional work by the AFRL has focused on segmented mirror spacecraft technologies in the 2002 Deployable Optical Telescope (DOT) project. DOT objectives focused on the capturing and maintaining phasing between multiple segments to ensure proper segment alignment, effectively creating a single large diameter mirror (Lane & Lacy, 2008, p. 568). An optical vibration control design process suggested by Dr. Adam Yingling from his NPS SMT laboratory research is depicted in Figure 3, with the red blocks indicating Yingling's focus area. As shown, the structural model (design step 5) is a gateway to the development of mathematical models for dynamic control in an adaptive optics system. As segmented mirror systems require complex structure to remain lightweight, the structural model is often equally complex and can be inefficient for performing dynamic analysis. Therefore a technique to allow efficient and accurate analysis solutions is desired.

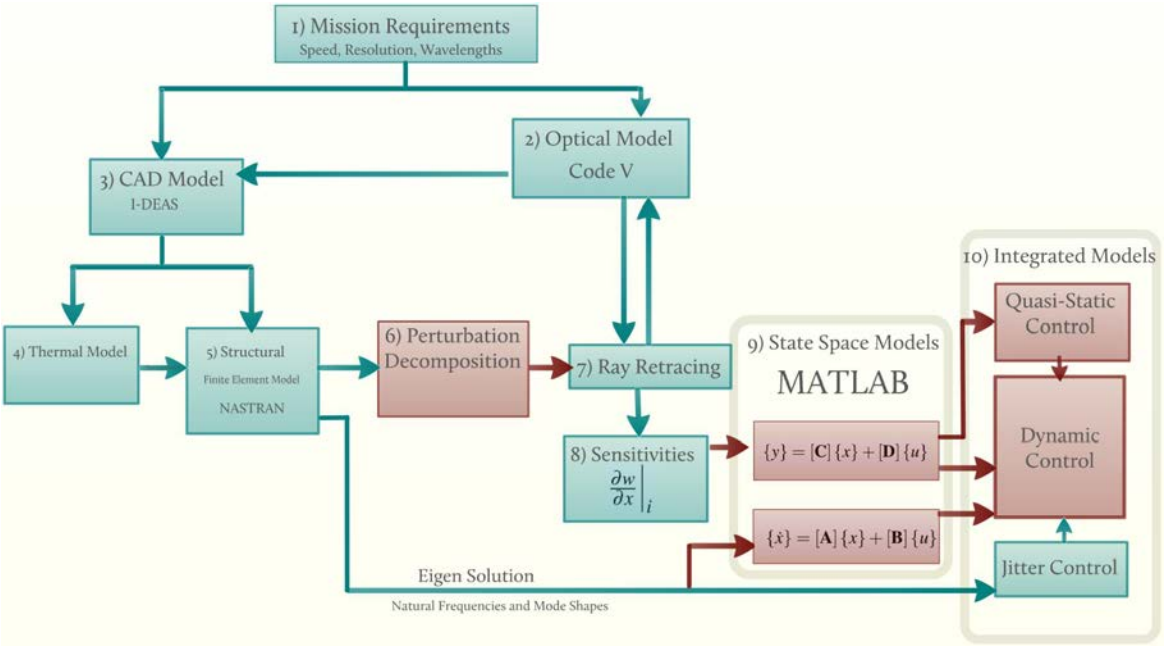

Figure 3. Integrated design process for SMT systems (Yingling, 2012, p. 15)

Superelement Partitioning Technique

The use of the external superelement technique for analyzing large finite element models is frequently implemented to both reduce simulation run times as well as allow analytical solutions be obtained with minimal computer resources. This technique is described in detail by Zu-Qing Qu's text, "Model Order Reduction Techniques" and can be used for analysis of both static and dynamic problems. External superelements represent groups of elements within the model which are condensed into a single element, analyzed independently, and assembled into a reduced model for subsequent analysis. A linear system can be represented by a 2nd-order equation of motion (EOM) with mass (M), proportional damping (C), and stiffness (K) matrices, x being the degree of freedom of the model, and F used for a forcing excitation, written as shown in Equation (2).

$$[\mathrm{M}]\{\ddot{x}\} + [\mathrm{C}]\{\dot{x}\} + [\mathrm{K}]\{x\} = \{F\} \tag{2}$$

The eigenvalue of K in the space of M gives the mode shapes with the eigenvalue used to calculate the vibration natural frequencies. By partitioning each substructure EOM by internal slave (s) and boundary master (m) dof, a partitioned substructure can be written as shown in Equation (3).

$$\begin{bmatrix} M_{mm} & M_{ms} \\ M_{ms}^{\ T} & M_{ss} \end{bmatrix} \begin{Bmatrix} \ddot{\vec{x}}_m \\ \ddot{\vec{x}}_s \end{Bmatrix} + \begin{bmatrix} C_{mm} & C_{ms} \\ C_{ms}^{\ T} & C_{ss} \end{bmatrix} \begin{Bmatrix} \dot{\vec{x}}_m \\ \dot{\vec{x}}_s \end{Bmatrix} + \begin{bmatrix} K_{mm} & K_{ms} \\ K_{ms}^{\ T} & K_{ss} \end{bmatrix} \begin{Bmatrix} \vec{x}_m \\ \vec{x}_s \end{Bmatrix} = \begin{Bmatrix} {}^{I}F_m \\ 0 \end{Bmatrix} + \begin{Bmatrix} {}^{E}F_m \\ 0 \end{Bmatrix} \qquad (3)$$

Master nodes represent connection points between superelements and the remaining structure as well as locations of constraints and externally applied forces (${}^{E}F_m$). For static analysis, the Guyan Condensation method can be implemented to omit interior slave dof which produces exact solution reduced EOM matrices. For dynamic analysis, Guyan Condensation produces an exact stiffness matrix, but the mass and damping matrices are approximated (inertia/local dynamic effects ignored). Hence this method is valid only for very stiff components and modal frequencies ranging up to $0.3\lambda_c$, where the cutoff eigenvalue λ_c (or cutoff frequency, ω_c) is the lowest eigenvalue computed with the slave model (Qu, 2004, pp. 80-81). The slave model is the full model with all master node dof fixed. Guyan Condensation is an extremely efficient method for performing the required matrix reduction but the associated dynamic analysis errors are not acceptable for a model with nanometer level sensitivity. An alternative method is to use Dynamic Condensation (also known as Component Modal Synthesis) in which the eigen solution of the resulting reduced model exactly replicates dynamics of the full model (Qu, 2004, p. 79). During condensation, internal displacements within the superelements are translated to the master nodes through internal forces ${}^{I}F_m$. Degrees of freedom associated with the superelements can then be removed from the model leaving

the residual structure as a reduced model. Regions of interest, such as mirror segments in this application, must remain as residual structure. The reduced model can then be written as shown in Equation (4), with M_R, C_R, and K_R representing the residual structure matrices.

$$[M_R]\ddot{\vec{x}}_m + [C_R]\dot{\vec{x}}_m + [K_R]\vec{x}_m = \left\{ {}^{I}F_m \right\} + \left\{ {}^{E}F_m \right\} \tag{4}$$

With a reduced model, traditional FEA methods can be used and solutions obtained at increased speed with less computing resources. The superelement partitioned EOM must be solved only once, then iterative tuning need only be performed with the residual structure.

Model Correlation and Tuning

An FEM must be tuned if system behavior predictions and reliable mathematical models for control systems are desired. In order to tune an FEM model, methods for comparing analytical results to experimental data is necessary. The simplest, direct comparison begins with matching natural frequencies by plotting FEM eigenvalue results versus experimental natural frequencies for all modes of interest. With a strong correlation between the result sets, the points will lie near a straight line. Points systematically diverging can be a good indicator for a poorly modeled characteristic of the system (Marwala, 2010, p. 33).

Further direct comparison can be performed by plotting the elements of each mode shape with the simulated eigenvectors, again looking for a straight line (with slope equal to one if mass normalized). Wide scattering of points are an indicator the mode shapes under comparison do not correspond to the same mode (Marwala, 2010, p. 34).

The superelement partitioning of the SMT, along with further model reduction by decreasing model complexity, is detailed in Chapter III. Additionally, the methodology to obtain SMT dynamic response data for model correlation and tuning is presented.

III. Methodology

High-Fidelity Finite Element Model (HiFi-FEM)

Finite element models are used to capture deflections and dynamics of complex structures by approximating them with a set of interrelated small linear elements. All analysis done in this work is linear, as justified by the small amplitude displacements when in operation. By considering the mass distribution and the relative stiffness of adjacent nodes, the vibration mode shapes can be determined. Many programs exist that handle the numeric challenges of performing the eigenanalysis of large systems. A NASTRAN compatible model was provided by NPS. The model consists of elements representing all the telescope optics and supporting structure with a high level of detail, shown in Figure 4.

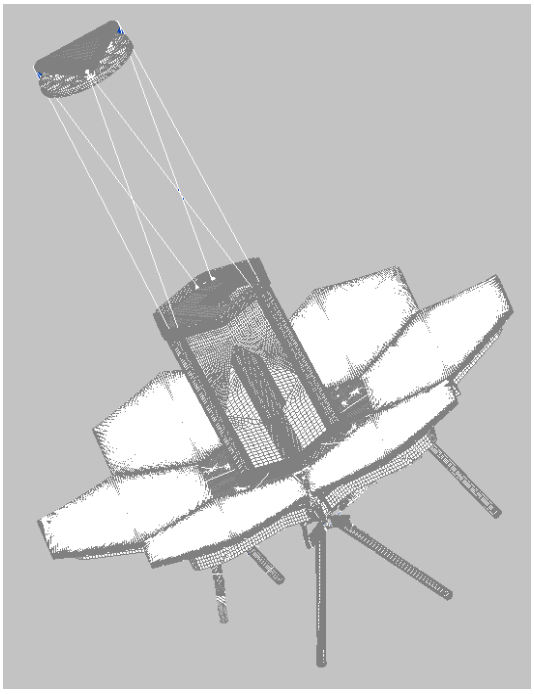

Figure 4. SMT high-fidelity finite element model

The boundary conditions consist of six isolator rods fixed at the base in all six dof. This accurately represents the mounting of the system to the adapter ring of its supporting structure, as shown in Figure 5.

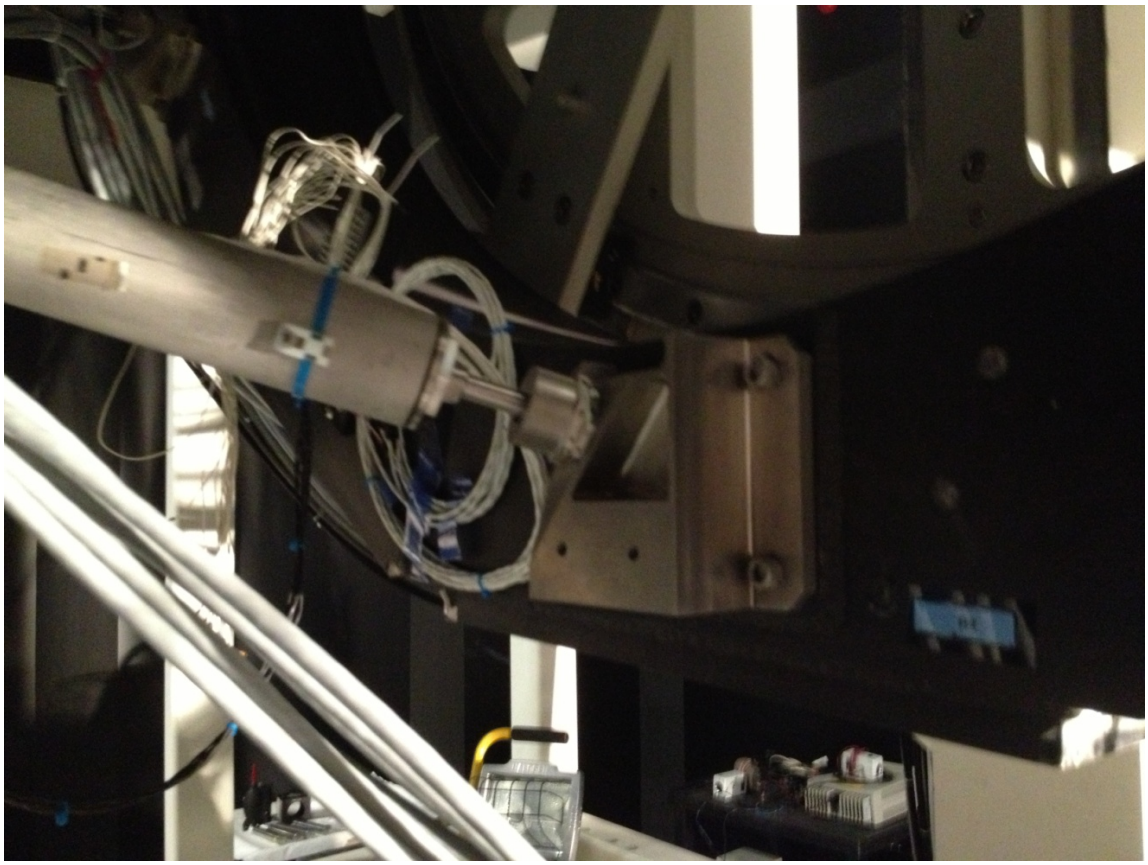

Figure 5. Isolator rod to adaptor ring joint fixed boundary condition

The FEM includes mass, spring, laminate, and rigid elements in addition to the structural elements. The spatial resolution is very high, resulting in 3.26 million dof. To obtain eigenanalysis solutions, using a clustered server for large memory allowances, the runs typically required 140 minutes for batches of ten modes. Even simple operations like model rendering were cumbersome, causing concern for the planned iterative model tuning schemes initiated in this research.

SMT Modal Testing

From analysis performed with the HiFi-FEM, a prediction of global and local segment mode shapes were obtained and used to design a test plan for modal experimentation on the SMT. Previous laser vibrometer testing was conducted by the Air Force Institute of Technology (AFIT) in December 2011. The previous testing focused on the low frequency (25 - 45 Hz) global modes and captured limited data on the high frequency (150 - 500 Hz) local segment bending modes, with displacement amplitudes between 0.5-1 nm (Jennings & Cobb, 2013). The experimental setup used is shown in Figure 6.

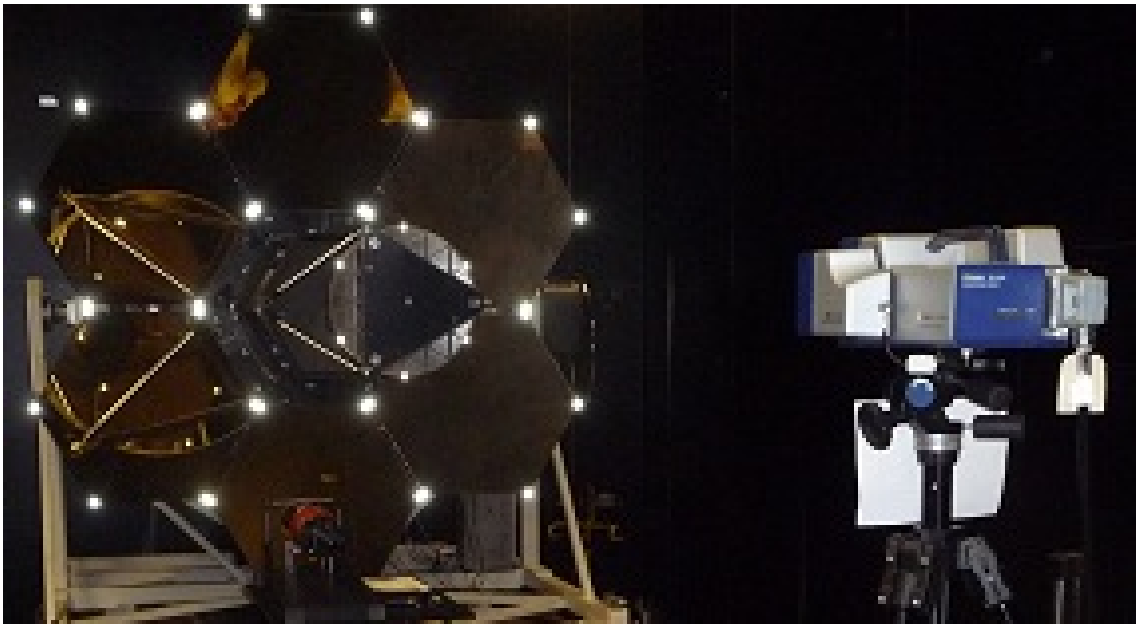

Figure 6. 2011 laser vibrometer data collection (Jennings & Cobb, 2013, p. 4)

The SMT resides within a laboratory susceptible to acoustic reverberation. During modal testing, acoustic disturbances can cause considerable signal noise during vibration measurements. As this experiment relied primarily on ambient acoustic waves as the excitation source (low coherence stemming from low signal-to-noise ratio (SNR)

and fluctuating background acoustic disturbances during the lengthy 3.25 hour experiment runs) data quality was less than ideal, particularity for the high frequency modes (Jennings & Cobb, 2013, p. 14). A summary of the findings from previous testing is included in Chapter IV.

Due to the low coherence values during previous testing for the local segment bending modes, additional testing was performed in September 2013, with alternate excitation sources to improve both the signal-to-noise and input signal quality. A Polytec PSV 400 scanning laser vibrometer with an OFV-5000 controller and signal analyzer was used. This allowed high spatial density response sensing across the segment surfaces allowing accurate estimation of the operational mode shapes. For computing frequency response functions (FRF), a reference laser signal, aligned to a corner reflector of the segment under test, was used. As conclusive data on the lower frequency global modes was previously obtained, modal testing focused on the high frequency (150 – 500 Hz) local segment bending modes in which the FEM predicted significant out-of-plane displacements. The experimental setup is shown in Figure 7.

The SMT laboratory is inherently a noisy environment. Therefore an increased input signal was used, giving greater SNR and allowing more precise analysis of dynamic characteristics for FEM tuning. To achieve this, compact proof mass actuator (PMA) shaker was installed on a segment's petal support structures as the excitation source. The shaker replaced one of two tuned mass damper (TMD) previously installed to dampen fundamental frequencies below 30 Hz.

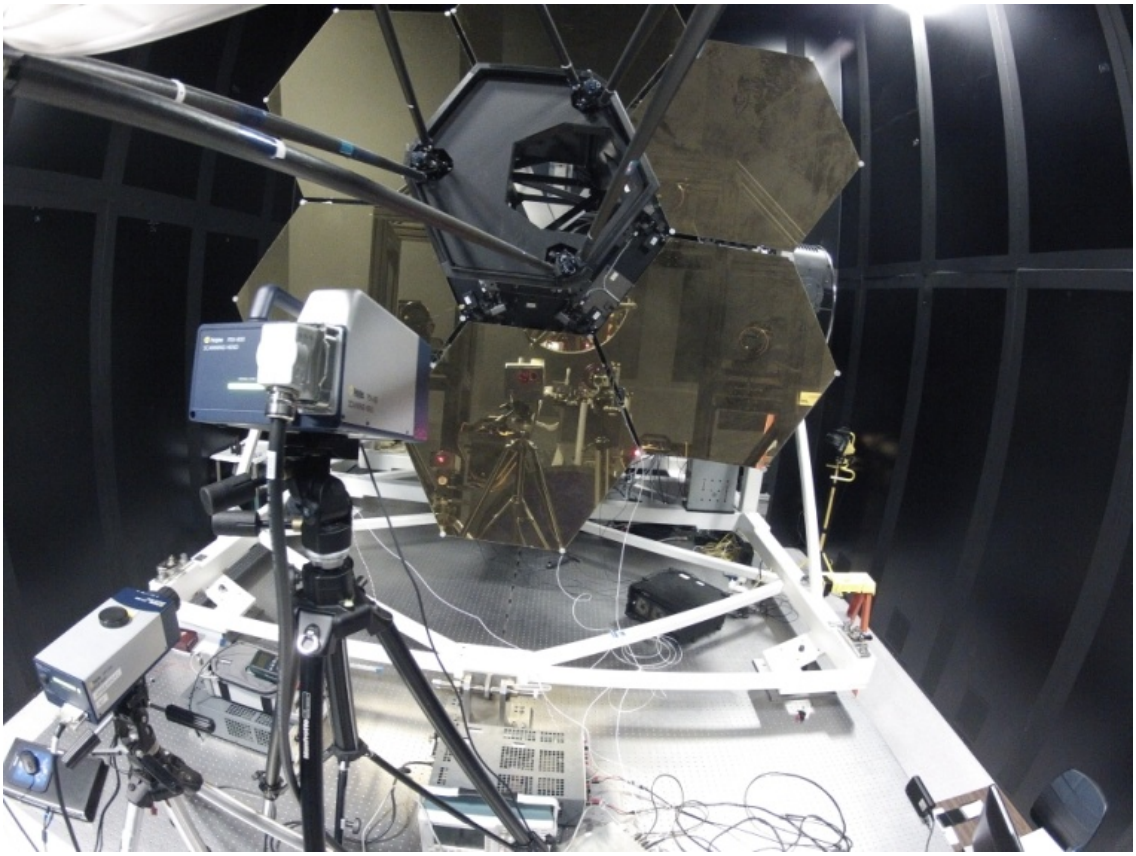

Figure 7. September 2013 laser-Doppler vibrometer data collection

The shaker was of similar size and weight of the replaced TMD. The replaced TMD and a shaker to TMD comparison is shown in Figure 8. The baseline test configuration involved replacing one TMD with the PMA shaker device. Alternate configurations were also tested. A “3 TMD equivalent” configuration involved leaving both TMDs in place and installing the shaker in the center position. A “1 TMD equivalent” involved removing both TMDs and installed the shaker in the center position.

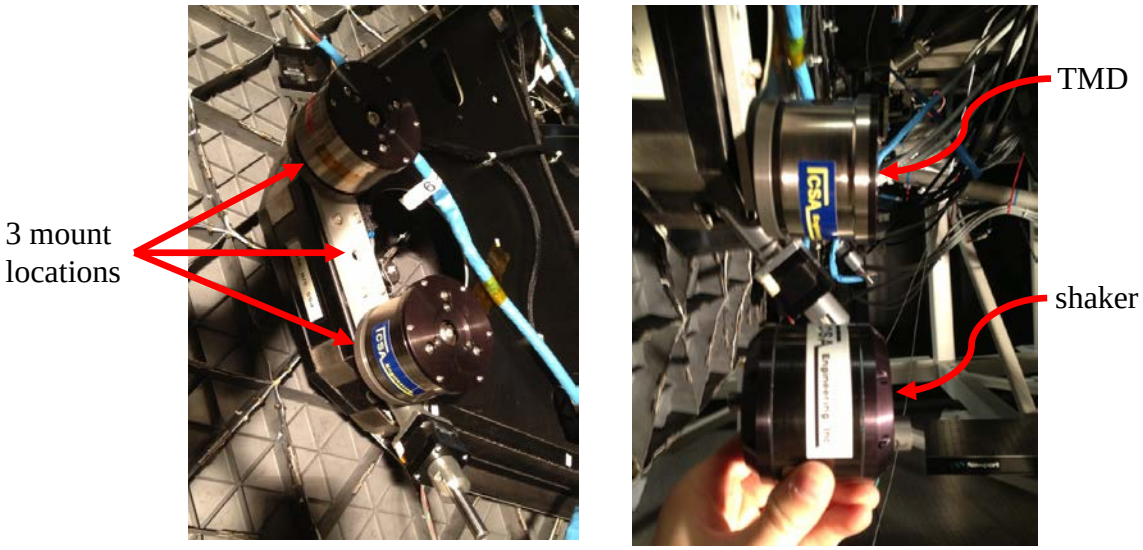

Figure 8. TMD locations and shaker comparison

Up to 61 locations along the mirror segment surfaces were scanned in order to obtain precise out-of-plane shapes of the segment bending modes. Additionally, impact hammer tests were conducted, with input strikes at the segment support FCAs, see Figure 9, and up to 31scan locations on the segment surface. The scan grid for both shaker and hammer tests is shown in Figure 10.

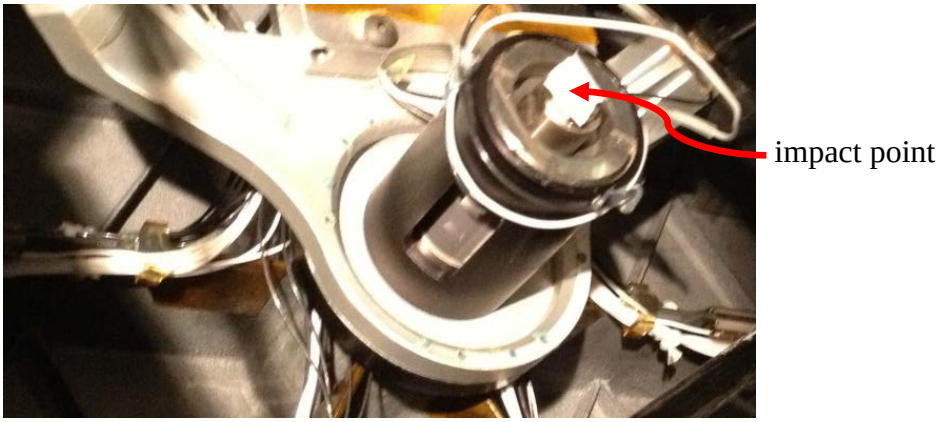

Figure 9. Impact hammer strikes to FCA for direct excitation input to segments

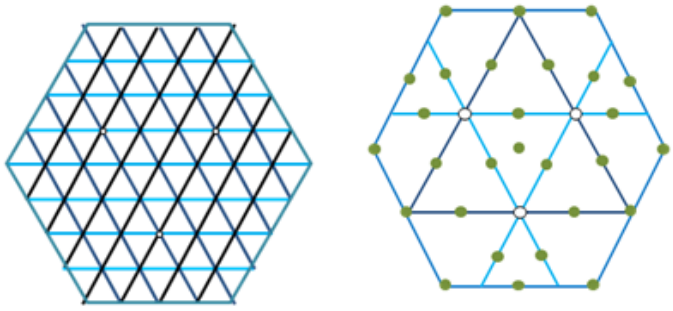

Figure 10. Modal test scan point grid (shaker = 61 points / hammer = 31 points)

For all test runs, the frequency bound was set to 1000 Hz, with a resolution of 0.625 Hz during the shaker runs and 1.25 Hz during the impact hammer runs. The data was processed using five averages and no overlapping. No window was needed during the shaker runs as a burst chirp signal was used. A diagram showing an overview of the test setup is given in Figure 11. Multiple references (laser reference and accelerometer references) were used to allow separation of possible repeated (pseudo-repeated) modes due to the symmetry of the hexagonal segments.

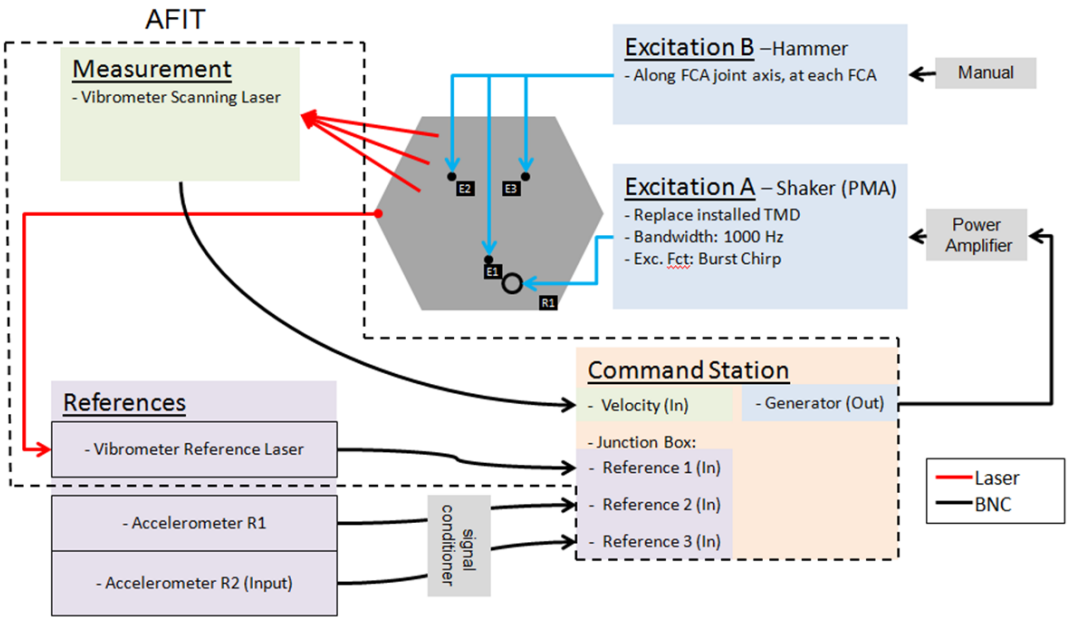

Figure 11. Experimental setup overview

Scan times for each run ranged from 10 to 20 minutes for each mirror segment, with data collected on segments 4, 5, and 6, numbered as shown in Figure 12. Two setup runs were performed, followed by nine shaker runs and nine hammer runs. Results from the modal testing are presented in Chapter IV.

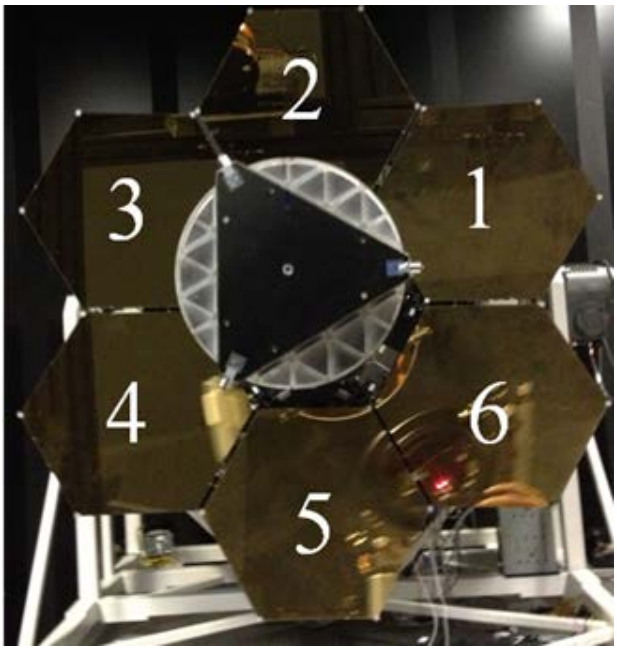

Figure 12. Segment numbering scheme

Superelements, Substructuring the SMT FEM

To meet the objective of creating a more efficient SMT FEM, model substructuring and the use of fewer elements in key components was implemented. As discussed in Chapter II, the use of superelements in a FEM can dramatically improve model efficiency and flexibility. To implement this technique, clear goals for FEA must be established and specific regions of interest within the model must be identified. Next, interfaces and joints between this region of interest and the remaining structure are identified. Finally, substructures are partitioned apart from the model as superelements leaving only the region of interest remaining as the residual structure.

For the SMT, knowledge of the dynamic behavior of the primary mirror to disturbance is essential to creation of a control system to reduce or eliminate image jitter. Therefore the six primary mirror segments were classified as residual structure, as defined in Chapter II. The secondary mirror and central hexagonal support structure were also included as residual structure. The secondary mirror is included as a region of interest as it was shown in early system testing that the tower supporting this mirror is susceptible to large amplitude motion during low frequency disturbances. The central hexagonal support structure was found to be a critical interface between the primary mirror segments and the remaining structure. Including this central support as residual structure simplifies partitioning the remaining structure into superelements. A diagram depicting the FEM partitioning into single-level superelements is shown in Figure 13. A graphical view of the superelement partitioned FEM is shown in Figure 14.

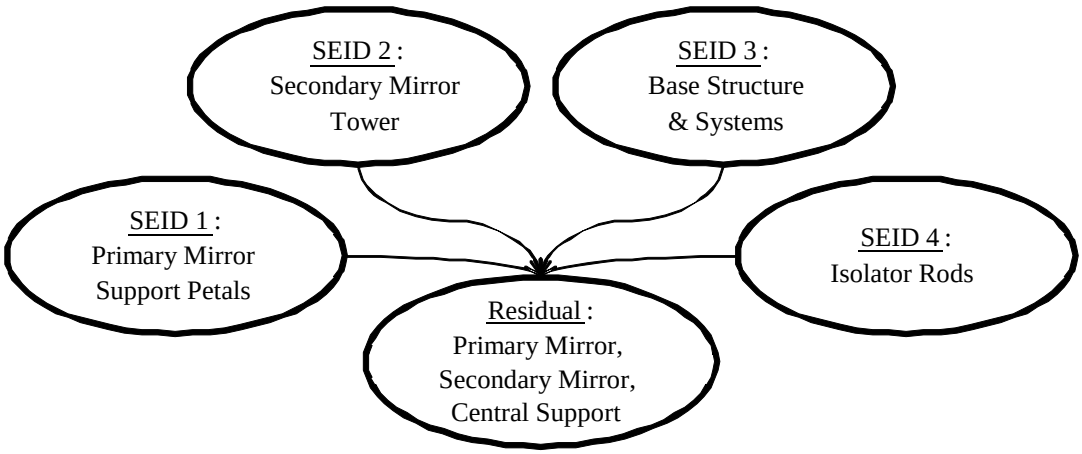

Figure 13. SMT FEM single-level substructuring scheme

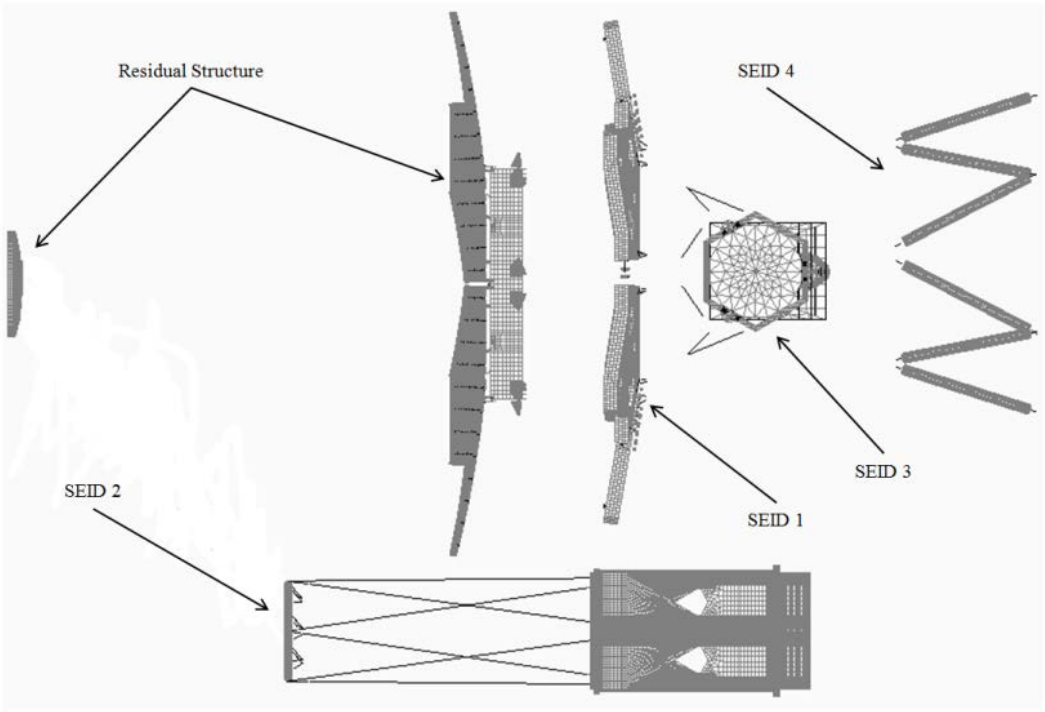

Figure 14. SMT FEM substructuring, graphical view

Superelement 1 consists of the segment petal support structure, including the elements representing the CCA and FCA flexures. The secondary mirror support tower is defined by Superelement 2. Superelement 3 includes all components and sensors in the optical drive train following the secondary mirror and supporting structure. Lastly, Superelement 4 defines the isolator rods that ground the SMT to an adaptor ring solidly fixed to an isolation table.

To determine FEM dynamics, a modal analysis is performed on each superelement independently, requiring on average of 4 minutes/superelement on a standard equipped desktop computer (2.7 GHz dual processor, 4GB RAM). Then, solving the EOM iteratively need only be performed on the residual structure with 1.49 million dof (over 45% reduction in dof compared to the HiFi-FEM). A detailed list of the residual and superelement interface (master) nodes can be found in Appendix A.

Reduced-Order Mirror Segment Modeling (RO-mirror)

Beyond partitioning the HiFi-FEM into superelements, further improvements in model efficiency was possible by reducing the complexity of the residual structure. With 35% of the nodes/elements of the HiFi-FEM being used for modeling the primary mirror segments, large gains in analysis run times could be achieved by creating a reduced-order mirror segment (RO-mirror) to replace the six high-fidelity segments (HiFi-mirror) in the original model.

Each segment originally included plate, laminar plate, bars, solids, and rigid elements. The plate elements were used to model the non-uniform isogrid substrate (deeper isogrid web walls near the mirror edges). The segment surfaces were comprised of a three layer laminar plate elements. The bar, solid, and rigid elements composed the three joint interfaces between the segment and FCAs supported by the petal support structure. Three views of the HiFi-mirror are shown in Figure 15.

To reduce the complexity of the segments, a common technique is to model uniform isogrid panels with a single flat plate and adjust the material Young's Modulus (E) and thickness (t) with equivalent values (E* and t*). This method, originally developed by NASA in 1973 (McDonnell Douglas Astronautics Company, 1973), was established to allow for more efficient load analysis of geometrically complex panels/plates. This technique can be applied to isogrid panels using appropriate geometric parameters and "will give the same bending and extensional stiffnesses" as that of the original isogrid panel (McDonnell Douglas Astronautics Company, 1973, p. 32).

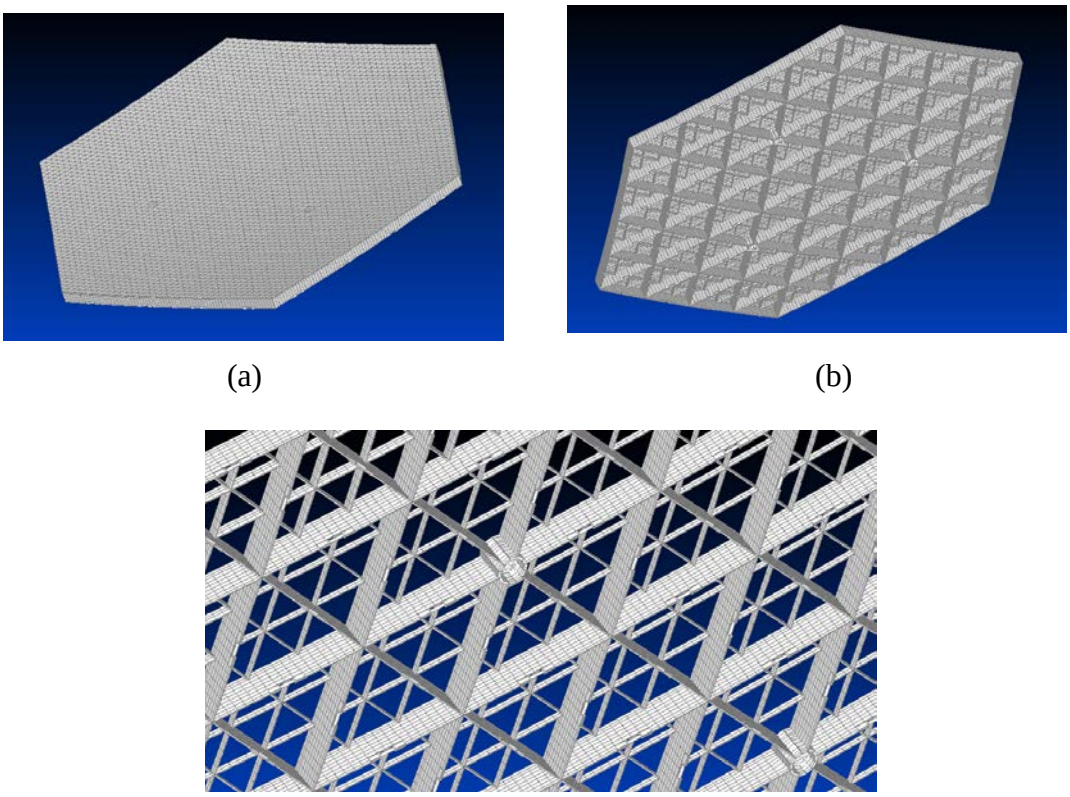

(a) (b)

(c)

Figure 15. HiFi-mirror: (a) top, (b) bottom, (c) isogrid substrate

The theory and experimentally validated equivalency equations assume a uniform isogrid, as well as the same material properties for the face sheet as the isogrid substrate. Since the SMT isogrid is not uniform (three unique web depths: 2, 3, and 9 units) and consists of varying materials between the face sheet and substrate, the most accurate results were found by separating the equivalent plate into two layers. The top layer (Layer1) models the segment face sheet and substrate isogrid web depths (6 units along outer edges, 7 units on interior). The bottom layer (Layer2) models only substrate web depths not accounted for in the base isogrid (3 units along outer edges, 2 units on interior). To model this non-uniform isogrid, the layers were meshed with unique material properties for the outer versus the inner plate elements, making a total of four

E*/t* material property cards. The face sheet was included in the Layer1 calculations. Since the thickness of the face sheet is in the denominator of the NASA calculations, a solution for the Layer2 properties, without a face sheet, was possible by taking the limit of the solutions as the thickness approached zero. The layers were then offset from each other based upon moment of inertia calculations to preserve flexural rigidity. A depiction of the two-layer RO-mirror is shown in Figure 16, with the center elements hidden and an exaggerated offset for clarity. As can be seen, the parabolic curvature from the HiFi-mirror was retained in the RO-mirror model. Many attempts at simpler equivalent plate models were conducted with the results of each method presented in Chapter IV.

Parabolic (midside nodes) triangular plate elements, with twelve elements per free edge, were used in the reduced-order mesh. This element sizing matches the actual isogrid sizing and allowed easy insertion of the RO-mirror into the model residual structure as mirror-to-petal joints are located at isogrid intersections. Three mass elements were used to replace the many bar, solid, and rigid elements originally used to model the segment-to-petal joint structure.

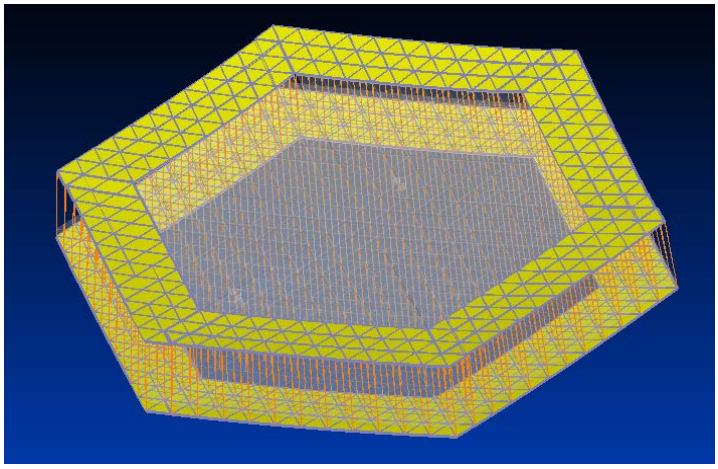

Figure 16. RO-mirror segment (exploded view)

Integration of the RO-mirrors

When creating the RO-mirror model, comparisons between a simplified segment and the HiFi-mirror were conducted with the three interface joints constrained as fixed in all six dof. While this allowed high precision refinement of the RO-mirror, all dynamics occurring between the petal support structure and the segment were lost. Integration of the RO-mirror back into the residual structure of the HiFi-FEM allows analytical solutions which capture both the global modes (particularly segment tip/tilt and piston motion relative to each other and to the secondary mirror) as well as the local segment bending modes. Achieving a reduced-order superelement FEM (ROSE-FEM) was completed by replacing the six HiFi-mirror segments in the residual structure with RO-mirror segments.

Initial Tuning – Direct Comparison Single Response Characterization

Initial model tuning was conducted to minimize a simple objective function J, the difference between the experimental natural frequency (ω_n) and modeled eigenvalue (λ) for the first local segment bending mode as shown in Equation (5).

$$J = |\lambda - \omega_n| \tag{5}$$

This difference was used as the response variable for implementing analysis iterations based on the design of experiment methodology. This methodology aids to minimize the runs required during iterative adjustments to the model's design variables and allows for a determination of the appropriate model material property settings to better match the system's dynamic behavior.

A Face-Centered Cube Design (FCD) was setup with the four RO-mirror Young's Modulus properties as the independent design variables. The FCD allows efficient

characterization of the FEM in terms of the dependent response variable, J. This design assumes a 2nd-order model of the response is adequate and minimizes the prediction variance near the center of the experimental region (near the center point run, or nominal E* values used to create the RO-mirror). This design was chosen as it is very efficient (minimal runs required) for developing a 2nd-order response model and also places strict limits on the range of the design variables (i.e. restricts E to be ≥ 0 psi) (Myers, Montgomery, & Anderson-Cook, 2009, p. 313). The design variables (X1 through X4) were coded between (-1) and (1) as shown in Table 1. With four design variables (factors), 25 analysis runs were required with the design shown in Table 2. The prediction equation for this design has the form shown in Equation (6) with b_i representing the estimated model coefficients from the 25-run FCD.

$$\hat{J} = b_0 + \sum_{i=1}^{4} b_i X_i + \sum_{i=1}^{4} \sum_{j=2, j\neq i}^{4} b_{ij} X_i X_j + \sum_{i=1}^{4} b_{ii} X_i{}^2 \tag{6}$$

Table 1. Design variable coding for design of experiment system characterization

Layer1 Inner E* = 3,549,800 psi $0 \le E_1 \le 7,099,600$	$X1 = \frac{E_1 - 3549800}{3549800}$
Layer1 Outer E* = 4,319,700 psi $0 \le E_2 \le 8,639,400$	$X2 = \frac{E_2 - 4319700}{4319700}$
Layer2 Inner E* = 1,111,500 psi $0 \le E_3 \le 2,223,000$	$X3 = \frac{E_3 - 1111500}{1111500}$
Layer2 Outer E* = 1,111,500 psi $0 \le E_4 \le 2,223,000$	$X4 = \frac{E_4 - 1111500}{1111500}$

Table 2. FCD for tuning model design variables

	Coded Units				Natural Units (Young's Modulus, E)			
	X 1	X 2	X 3	X 4	Layer1 Inner	Layer1 Outer	Layer2 Inner	Layer2 Outer
Full Factorial	-1	-1	-1	-1	0	0	0	0
	1	-1	-1	-1	7099600	0	0	0
	-1	1	-1	-1	0	8639400	0	0
	1	1	-1	-1	7099600	8639400	0	0
	-1	-1	1	-1	0	0	2223000	0
	1	-1	1	-1	7099600	0	2223000	0
	-1	1	1	-1	0	8639400	2223000	0
	1	1	1	-1	7099600	8639400	2223000	0
	-1	-1	-1	1	0	0	0	2223000
	1	-1	-1	1	7099600	0	0	2223000
	-1	1	-1	1	0	8639400	0	2223000
	1	1	-1	1	7099600	8639400	0	2223000
	-1	-1	1	1	0	0	2223000	2223000
	1	-1	1	1	7099600	0	2223000	2223000
	-1	1	1	1	0	8639400	2223000	2223000
	1	1	1	1	7099600	8639400	2223000	2223000
Axial	-1	0	0	0	0	4319700	1111500	1111500
	1	0	0	0	7099600	4319700	1111500	1111500
	0	-1	0	0	3549800	0	1111500	1111500
	0	1	0	0	3549800	8639400	1111500	1111500
	0	0	-1	0	3549800	4319700	0	1111500
	0	0	1	0	3549800	4319700	2223000	1111500
	0	0	0	-1	3549800	4319700	1111500	0
	0	0	0	1	3549800	4319700	1111500	2223000
center point	0	0	0	0	3549800	4319700	1111500	1111500

Using the methods described in this chapter, extensive high frequency data of the SMT were collected on three of the six segments. In addition, it was possible to create a ROSE-FEM less than 1/12 the size of the HiFi-FEM. Results of modal testing, model reduction, system response characterization, and initial tuning is presented in Chapter IV.

IV. Results and Analysis

Reduced-Order Mirror Segment Comparisons

A single modeled mirror was separated for comparison to verify that a RO-mirror is functionally equivalent to the high-fidelity segment. Equivalence was determined in both the static and dynamic sense. Static equivalence was based on constraining two edges of the segment and applying a static load on the opposite corner. Displacements (u) across the surface were compared. Table 3, in order of progression of the modeling methods applies, uses results from the static load case for the various equivalency modeling methods that were attempted, such as number of layers, adjustments to the element sizing, and E*/t* equivalency theories. Elongation is the total displacement divided by the width of the mirror, and Angle is the angle between a line from the clamped edge to the undeformed load point and a line from the clamped edge to the deformed load point. All values shown in Table 3 are percent difference compared to the results of the same static load case analyzed with the HiFi-mirror.

Table 3. Effect of various assumptions in static load displacements

Method	u_1	u_2	u_3	Elongation	Angle
1-Layer, Big Triangles Only (NASA)	-15%	691%	-14%	-19%	-14%
1-Layer, Little Triangles Only (NASA)	506%	616%	493%	338%	495%
1-Layer, Adjust b & iterate (NASA)	24%	20%	25%	4%	25%
1-Layer, Adjust t & iterate (NASA)	-95%	-95%	94%	-93%	-94%
2-Layer (Gibson & NASA)	161%	171%	158%	6%	159%
3-Layer (Gibson & NASA)	-5%	1%	-6%	6%	-6%
2-Layer, 2nd Layer lim t→0 (NASA)	4%	4%	4%	2%	4%

As can be seen, the two layer method based upon NASA's E*/t* theory provided the best reduced-order solution for modeling the segment isogrid with only 4% error in displacements and angle. This demonstrated that the RO-mirror had comparable stiffness

as the high-fidelity segment as the load produces the same deflection on each. Comparable displacement contours were obtained when the static load case was applied to the HiFi- and RO-mirrors. Figure 17 shows the displacement contours in the three orthogonal directions and the total displacement contours for the HiFi and RO-mirrors. In each illustration, the left end is clamped, and the load applied to the right vertex.

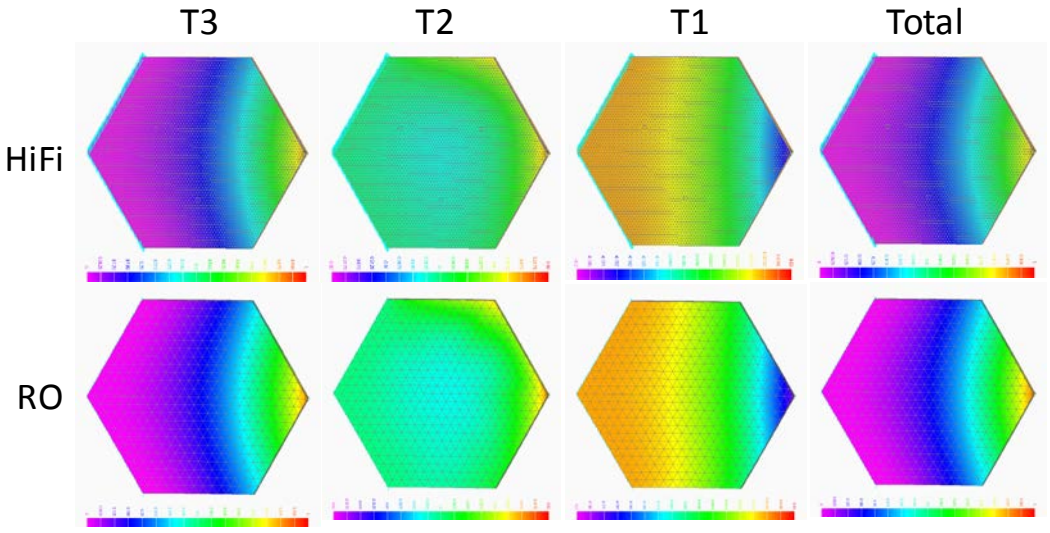

	u_1	u_2	u_3
Hifi Mirror	0.1702	-0.01481	-0.8549
RO Mirror	0.1763	-0.01547	-0.8858

Figure 17. Mirror static displacement (inches) comparison, HiFi- vs. RO-mirror

The RO-mirror mass and moment of inertia properties compared closely to the HiFi-mirror. The total mass of the RO-mirror is less than one-thousandth of a slug ($lb_f \cdot s^2/ft$) greater than the HiFi-mirror. Table 4 shows a comparison of mass properties with masses measured in slugs and center of gravity (CG, inches) relative to the center of a six segment primary mirror array.

Table 4. RO-mirror mass (slugs) and CG (inches) comparison

	Elements	Structural Mass	Non-Stru Mass	Total Mass	X-C.G.	Y-C.G.	Z-C.G.
HiFi-mirror	44,736	0.428	0.101	0.529	39.678	0.003224	4.707
RO-mirror	1,728	0.428	0.101	0.529	39.638	0.003215	4.948
% Difference	-96.1%	0.0%	0.0%	0.0%	-0.1%	-0.3%	5.1%

The moment of inertia properties of the RO-mirror were all within 5% of the HiFi-mirror. Table 5 shows the comparison of inertial properties with units of inches^4. Slight differences between the two mirror model CGs and inertial properties are an artifact of the E*/t* equivalency model reduction technique in conjunction with the parabolic shape of the primary mirror array (mirror segments are each tilted relative to the primary mirror central axis).

Table 5. RO-mirror inertial property comparison (inches^4, volume=inches^3)

	Ixx	Iyy	Izz	Ixy	Iyz	Izx	Volume
HiFi-mirror	2,392.4	30,199.8	31,694.2	2.25	0.3195	3,621.4	135.2
RO-mirror	2,278.8	28,990.4	30,332.4	2.17	0.3198	3,638.2	1,257.4
% Difference	-4.7%	-4.0%	-4.3%	-3.8%	0.1%	0.5%	830.1%

Dynamic equivalence was determined by a normal modes eigenanalysis. The three segment-to-petal support structure FCA joints were fixed. The four primary modes are shown in Table 6 comparing RO-mirror results to that of the HiFi-mirror, with experimental results for reference. With the nominal mass density properties, all the mode shapes agreed qualitatively. To allow direct comparison between mirror models, the four mass densities of the RO-mirror were adjusted to match the first eigenvalue of the HiFi-mirror. The mass densities were then reset to their nominal values before integration into the full FEM to ensure low frequency mode predictions from FEA of the full SMT model are unaffected by unrealistic inertial properties of the RO-mirror.

Table 6. RO-mirror dynamic comparison with experimental reference

RO-mirror	**Experimental**	**HiFi-mirror**
	Saddle Mode	
134.11 Hz 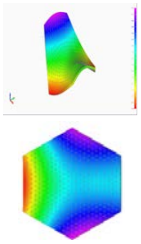	150 - 170 Hz 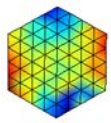	134.08 Hz 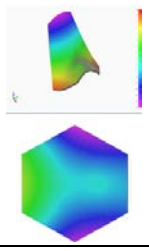
	Drum Mode	
201.63 Hz 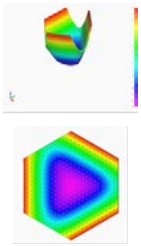	225 – 360 Hz 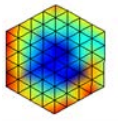	232.32 Hz 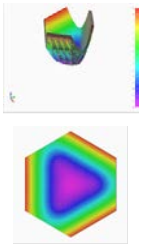
	Trefoil1 Mode	
304.72 Hz 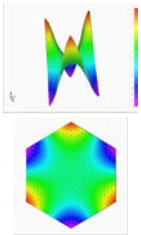	*275 – 345 Hz* 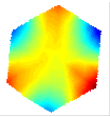	*322.29 Hz* 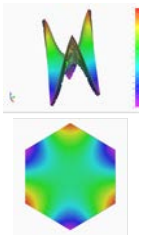
	Trefoil2 Mode	
368.76 Hz 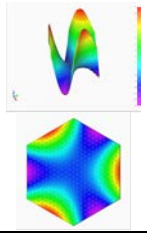	405 - 440 Hz 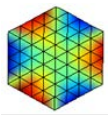	429.20 Hz 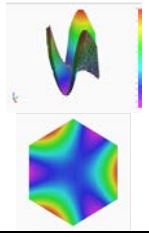

A comparison of frequencies between the HiFi- and RO-mirror models is shown in Figure 18. The RO-mirror model under predicted the frequencies of higher modes by approximately 12%, indicating the RO-mirror predicts lower segment stiffness.

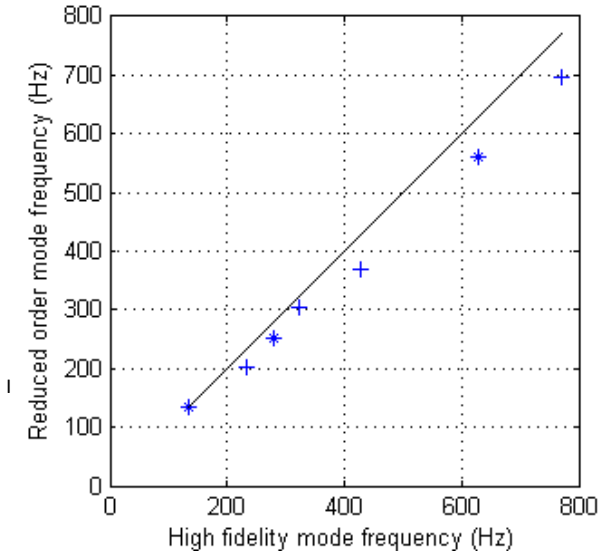

Figure 18. RO-mirror model under predicts higher frequencies. (* indicates 2 modes)

Reduced-Order Model Efficiency Gains

Using the two modeling approaches, superelement partitioning and E*/t* equivalency, considerable reduction in model size to the HiFi-FEM were possible. Figure 19 gives an overview of how each approach contributed to the creation of the final ROSE-FEM.

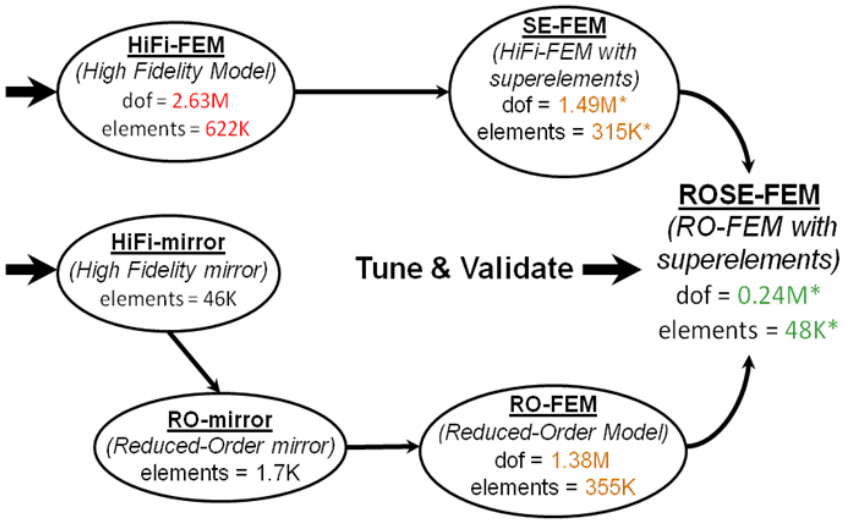

Figure 19. SMT FEM Reduction Overview (*does not include superelements)

A detailed comparison of model sizes, analysis run times, and computational memory required is presented in Table 7. Comparisons between the original HiFi-FEM, a reduced-order model with the RO-mirror segments (RO-FEM), the HiFi-FEM partitioned with superelements (SE-FEM), and ROSE-FEM are shown. All comparison solutions were obtained using MSC.NASTRAN on a Linux cluster node with 16 processors, 64 GB RAM, clocked on average over 400% real-time.

Table 7. FEA comparisons (*superelements require only 1 run)

	HiFi-FEM	**RO-FEM**	**SE-FEM**	**ROSE-FEM**
dof:	2.63 M	1.38 M	residual: 1.49 M	residual: 0.24 M
nodes:	589 K	340 K	residual: 292 K	residual: 43 K
elements:	622 K	355 K	residual: 315 K	residual: 48 K
Analyis run time: (1st 10 modes)	2:17:55	not available	SEID1: 07:25:38 SEID2: 14:29:09 SEID3: 05:42:31 SEID4: 00:08:22 **residual:** 00:31:37	*SEIDs **residual:** 00:16:54
Required file memory (GB): (1st 10 modes)	160	76	SEID1: 15 SEID2: 31 SEID3: 8 SEID4: 8 **residual:** 31	*SEIDs **residual:** 4

For all runs, elements representing hinges between pairs of petal supports were removed to be consistent with the current configuration of the SMT, shown in Figure 20. For the superelement partitioned analysis, superelement identifier (SEID) runs are sunk costs required only once. Additional tuning iterations require solutions be obtained for only the residual structure.

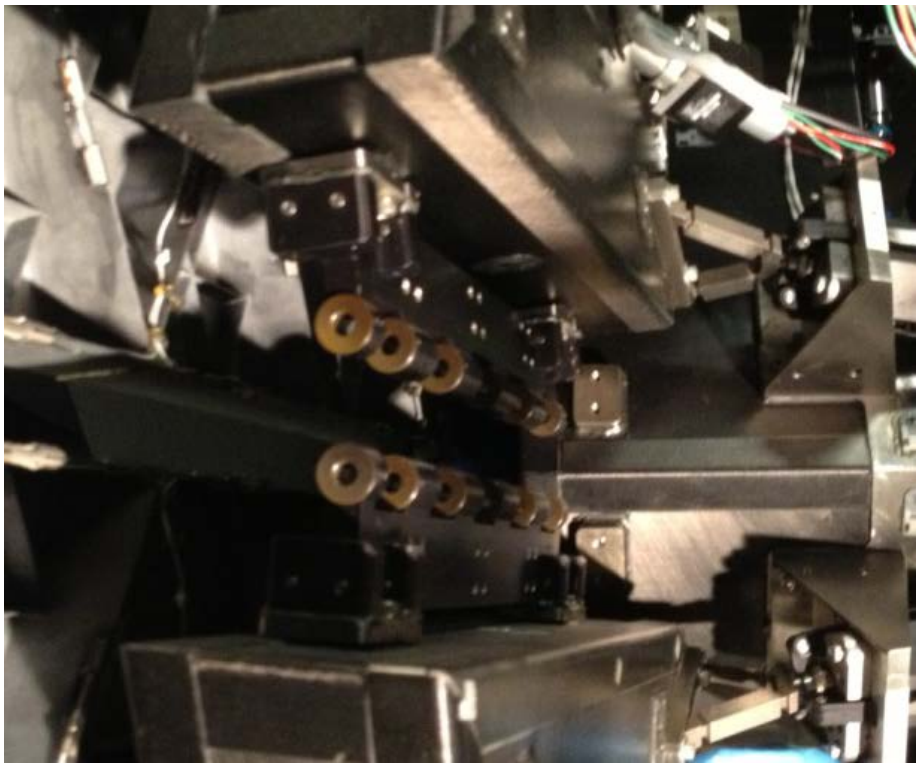

Figure 20. Petal support hinges removed in current SMT configuration

As shown, the combination of both superelement partitioning and isogrid equivalency model reduction methodologies yields substantial reduction in model size and efficiency. While a Linux cluster with unlimited virtual file memory was used to simulate all comparison runs, the superelement partitioned models have the advantage of requiring no more than 31 GB of temporary storage space. Because of this, analytical solutions could be obtained using a standalone desktop computer with limited memory.

All details regarding the superelement partitioning and isogrid equivalency modeling techniques used for the SMT FEM were presented in the conference manuscript titled "Model Complexity Reduction of a Segmented Mirror Telescope" by Dras, Jennings, and Cobb. The manuscript is included as Appendix B.

Modal Testing – Previous Vibration Measurements, Summarized

Previous laser vibrometer modal testing of the SMT found modes that can be grouped into three categories: frame modes, rocking modes, and curvature modes. The frame modes, occurring less than 20 Hz, consist of synchronous motion of all six segments described by global piston/tip/tilt movement. The rocking modes, occurring between 20 to 100 Hz, consist of local tip/tilts of individual segments. The curvature modes, occurring over 100 Hz, consist of out-of-plane bending of the segments. A depiction of these mode categories is given in Figure 21. The frequencies at which the low frequency modes occurred at are shown in Figure 22.

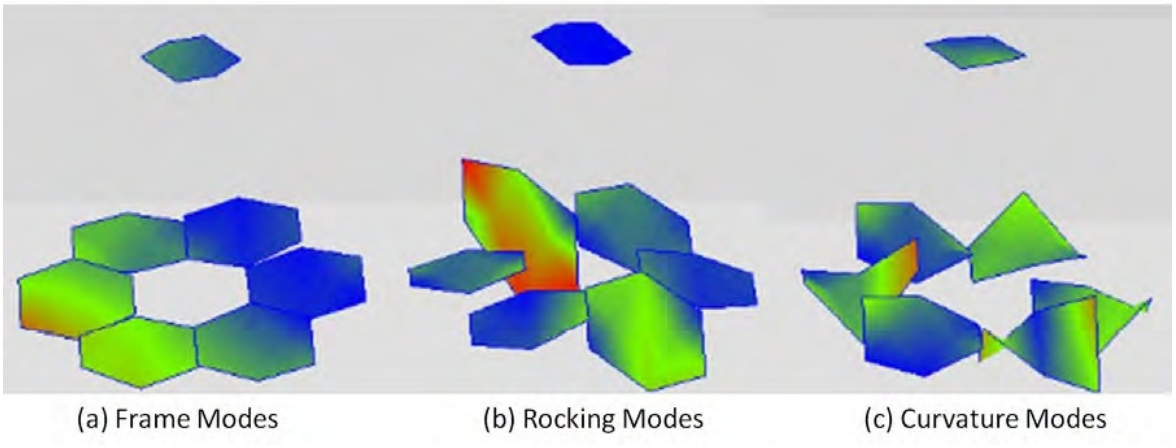

Figure 21. SMT dynamic mode categories (Yingling, 2012, p. 111)

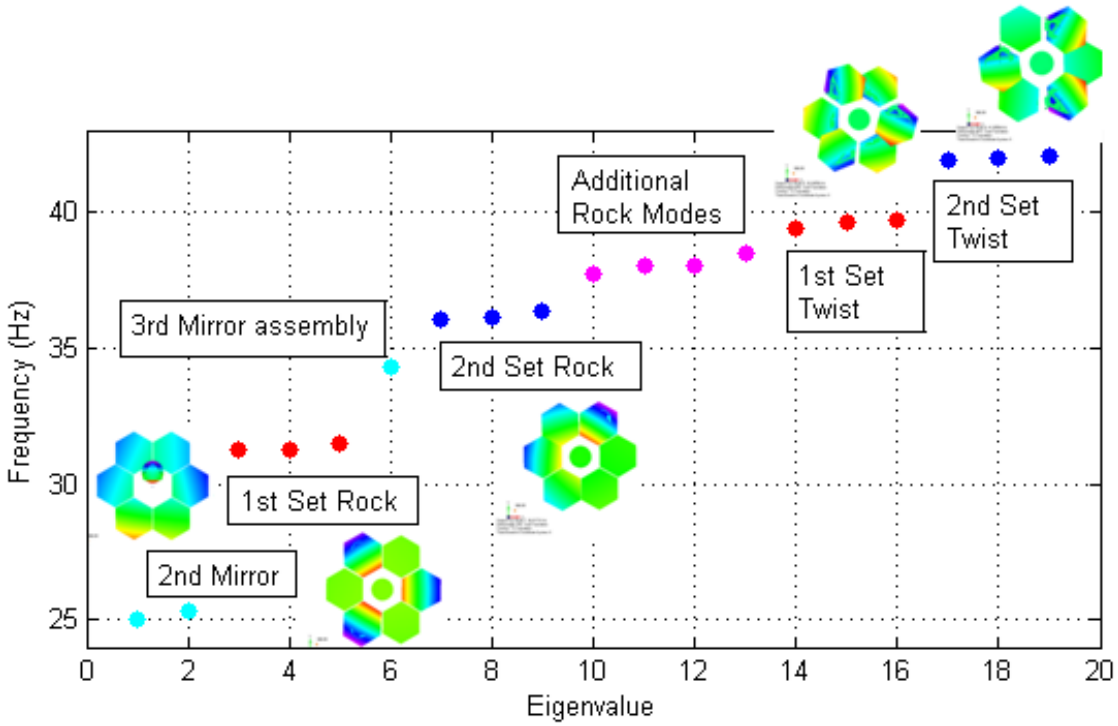

Figure 22. SMT low frequency modes (25 – 45 Hz) (Jennings & Cobb, 2013, p. 6)

The high frequency bending modes of the segments were seen experimentally in three distinct groups: saddle modes between 150 to 170 Hz (Figure 23), drum modes between 240 to 260 Hz (Figure 24), and a trefoil mode at 440 Hz (Figure 25). Considering each high frequency mode occurred at varying frequencies (within a 20 Hz band), it was determined small differences in symmetry exist despite identical segment designs. During model tuning, adjustments for each segment will be required to account for the fact that each segment's dynamic response is unique.

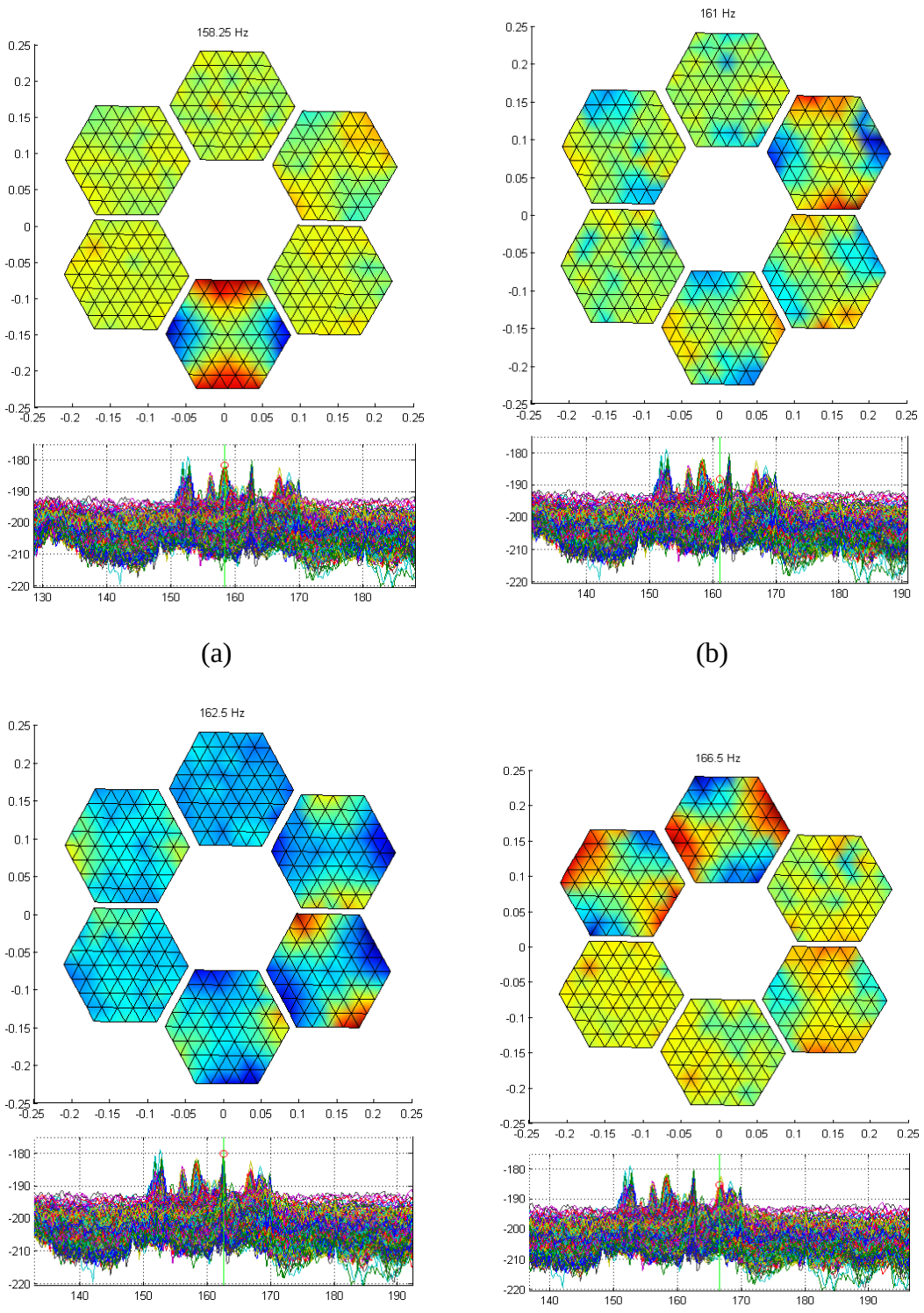

Figure 23. Saddle mode on all but segment 4: (a) 158.25 Hz, (b) 161 Hz , (c) 162.5 Hz, (d) 166.5 Hz (Jennings & Cobb, 2013, p. 10)

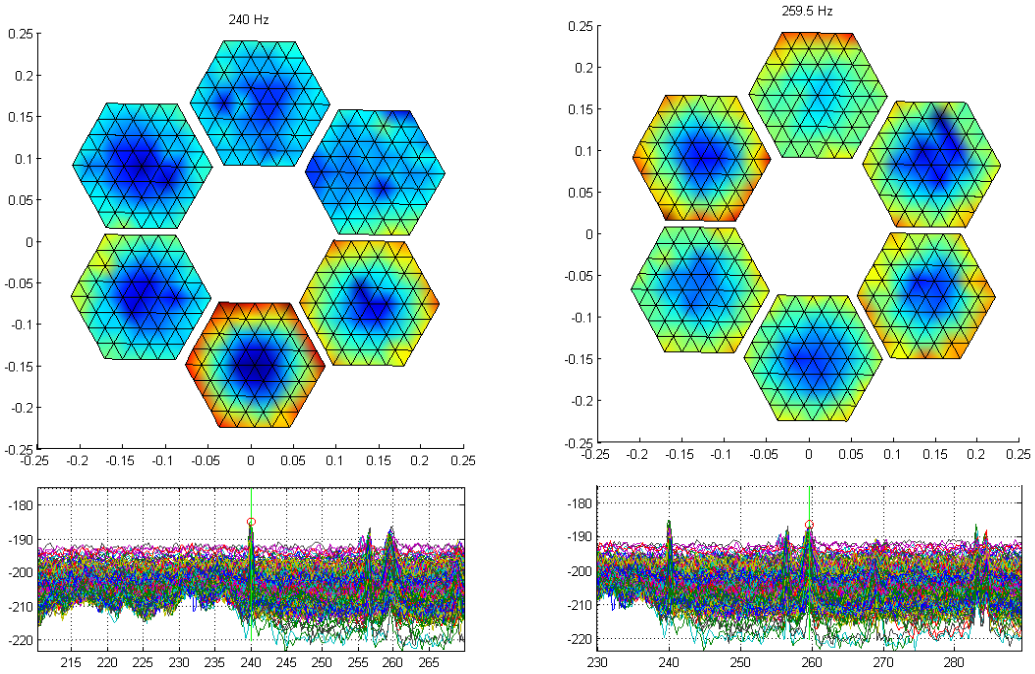

(a) (b)

Figure 24. Drum mode on all segments: (a) 240 Hz, (b) 259.5 Hz (Jennings & Cobb, 2013, p. 11)

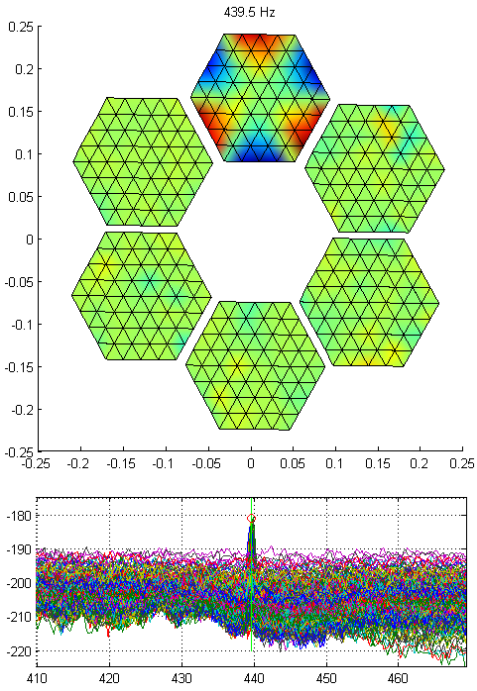

Figure 25. Trefoil2 mode, segment 2 only, 439.5 Hz (Jennings & Cobb, 2013, p. 12)

Modal Testing – Mirror Segment Vibration Measurements

Mirror segment modal testing concentrated on the high frequency segment bending modes between 120 to 500 Hz. The PMA shaker used as the excitation source was bench tested by directly fixing it to an isolation table to determine the FRF shown in Figure 26. The shaker device itself resonates at 182.5 Hz, but remains relatively stable in the frequency bands where segment resonances are expected to occur, 120 – 170 and 200 – 500 Hz.

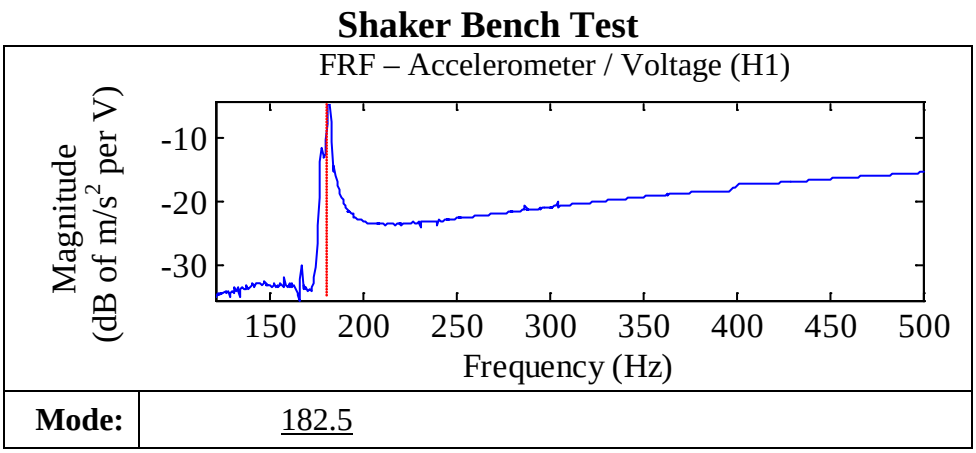

Figure 26. Shaker Bench Test FRF (121 – 500 Hz)

For testing individual segments, a baseline test configuration was established which involved replacing one of the two TMDs with the shaker device. In this configuration, inertial properties of the system remained nearly constant. Additional configurations were used to provide insight into the effect of the TMD masses to the high frequency modes. One of these configurations is referred to as "3 TMD equivalent" as both TMDs remained in place and the shaker was added in the center position. The "1 TMD equivalent" configuration involved removing both TMDs and using the shaker in the center position. Refer to Figure 8 for the placement locations. During segment 5 test

runs, additional data was collected in which the shaker was attached to adjacent segments (4 and 6) and responses measured from segment 5. While magnitudes of local segment 5 responses would diminish, it was expected that resonances associated with the petal support structure and segment-to-petal FCA joints would become more apparent.

Three test runs per segment were performed to collect impact hammer FRF data. For each run, hammer strikes to one of the three FCA allowed very strong input excitations into the segments. These runs are categorized as "right FCA, left FCA, and center FCA," with orientations as shown in Figure 27.

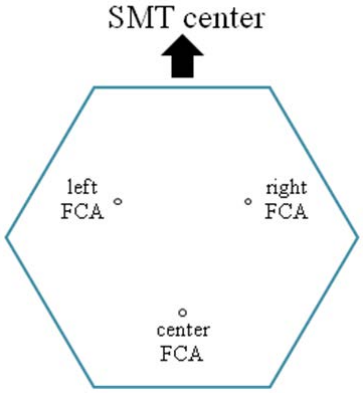

Figure 27. Impact hammer test FCA orientation

Modal Testing – Segment 4 Results

Modal testing of segment 4 produced good quality data with clearly discernible saddle and trefoil2 mode resonances. Of the 61 shaker test scan points, 51 were determined valid (i.e. acceptable SNR), while the hammer runs had 26 – 31 valid of the 31point grid.

FRF results, with plots showing maximum response, from all segment 4 tests are shown in Figure 28. Spectral lines are drawn in red to highlight mode resonances that were consistently excited. Black circles are drawn to indicate resonances that are

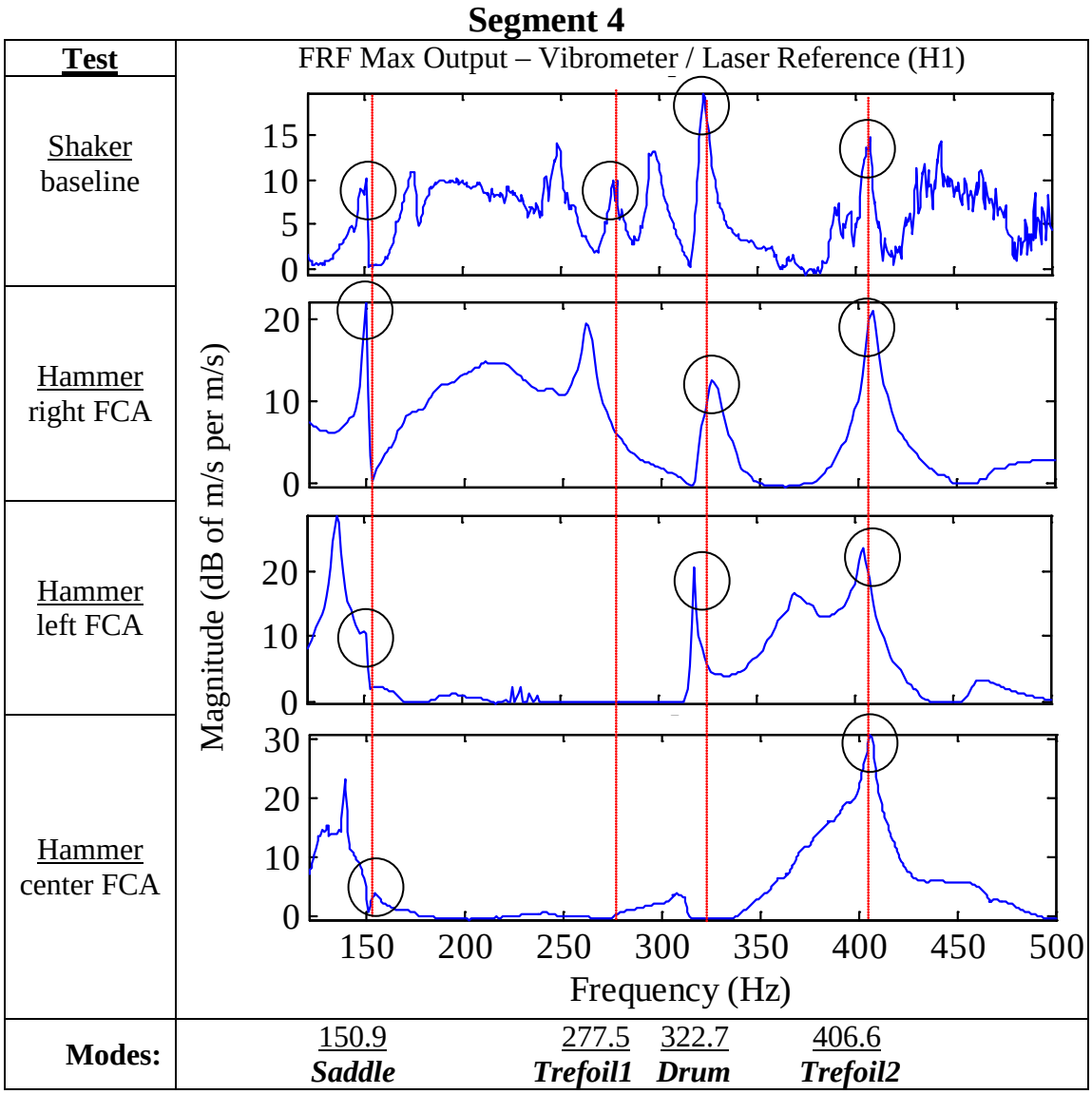

Figure 28. Segment 4 FRFs (121 – 500 Hz)

confirmed with mode shape contour plots, shown in Figure 29. The saddle mode for segment 4 was excited at approximately 151 Hz during all four runs. This saddle mode shape compares well to the ROSE-FEM predicted eigenvector contour plot. This mode was not excited during previous testing, but is easily discernible in the shaker and right FCA runs. The trefoil1 mode, for both segment 4 and 5, was not easily excited, but appeared around 278 Hz on segment 4.

Segment 4

FEM	*Shaker: baseline*	*Hammer: right FCA*	*Hammer: left FCA*	*Hammer: center FCA*
Saddle				
157.5719 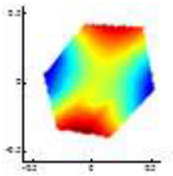	151.25 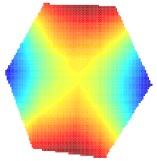	150.0 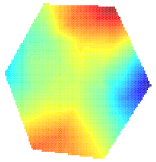	151.25 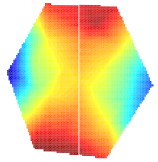	151.25 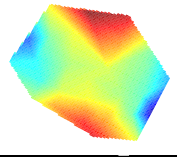
Trefoil1				
330.1313 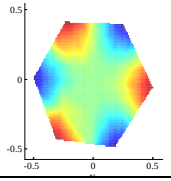	277.5 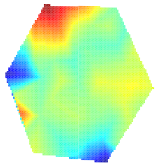			
Drum (and possible unique mode)				
300.106 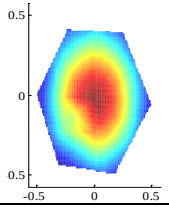	323.125 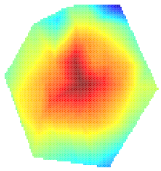	326.25 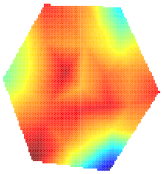	318.75 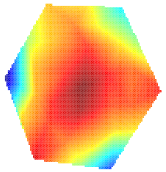	
Trefoil2				
383.3855 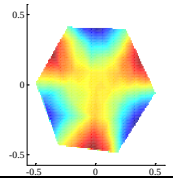	407.5 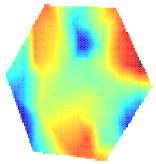	407.5 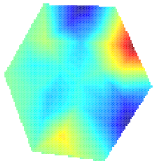	405.0 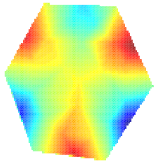	406.25 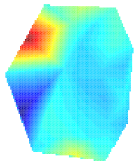

Figure 29. Segment 4 experimental mode shapes with FEM comparison

The drum mode appeared inconsistent across the three segment 4 runs with resonances near 323 Hz. The mode shapes obtained from hammer tests do not present as a drum shape but rather there seems to be swapping between a drum and Trefoil1 mode. The trefoil2 mode resonates strongly, around 407 Hz for segment 4, and showed consistent mode shapes during most all test runs of the three segments.

Using the half power method to determine frequency-dependent modal damping inherent in the segment, it was estimated the maximum damping is 0.8% occurring in the saddle mode (with no discernible difference between the various TMD test configurations),

Modal Testing – Segment 5 Results

Modal testing of segment 5 produced lower quality data than that of segment 4 and 6. While 60/61 scan points were accepted as valid during shaker testing, the shaker data is very noisy. During the center FCA runs, only 2/31 points were valid making it impossible to determine mode shapes accurately. For the two other hammer runs, 29/31 points were valid and resulted in very clean shape contours for the trefoil2 mode.

FRF plots for all segment 5 test runs are shown in Figure 30. Previous testing found a segment 5 saddle mode near 158 Hz with a well defined mode shape. The mode shape obtained from shaker tests, near 169 Hz, did not produce clear results, shown in Figure 31. Unique to segment 5, not predicted by the FEM, was an additional drum mode near 227 Hz similar to the finding during previous testing (segment 5 drum near 240 Hz). The expected drum mode occurred near 342 Hz and trefoil2 mode near 414 Hz. Both modes produced distinct mode shape contours. The trefoil1 mode was not excited during all segment 5 runs. Modal damping was estimated to be a maximum of 0.3%, occurring in the trefoil2 mode.

Segment 5

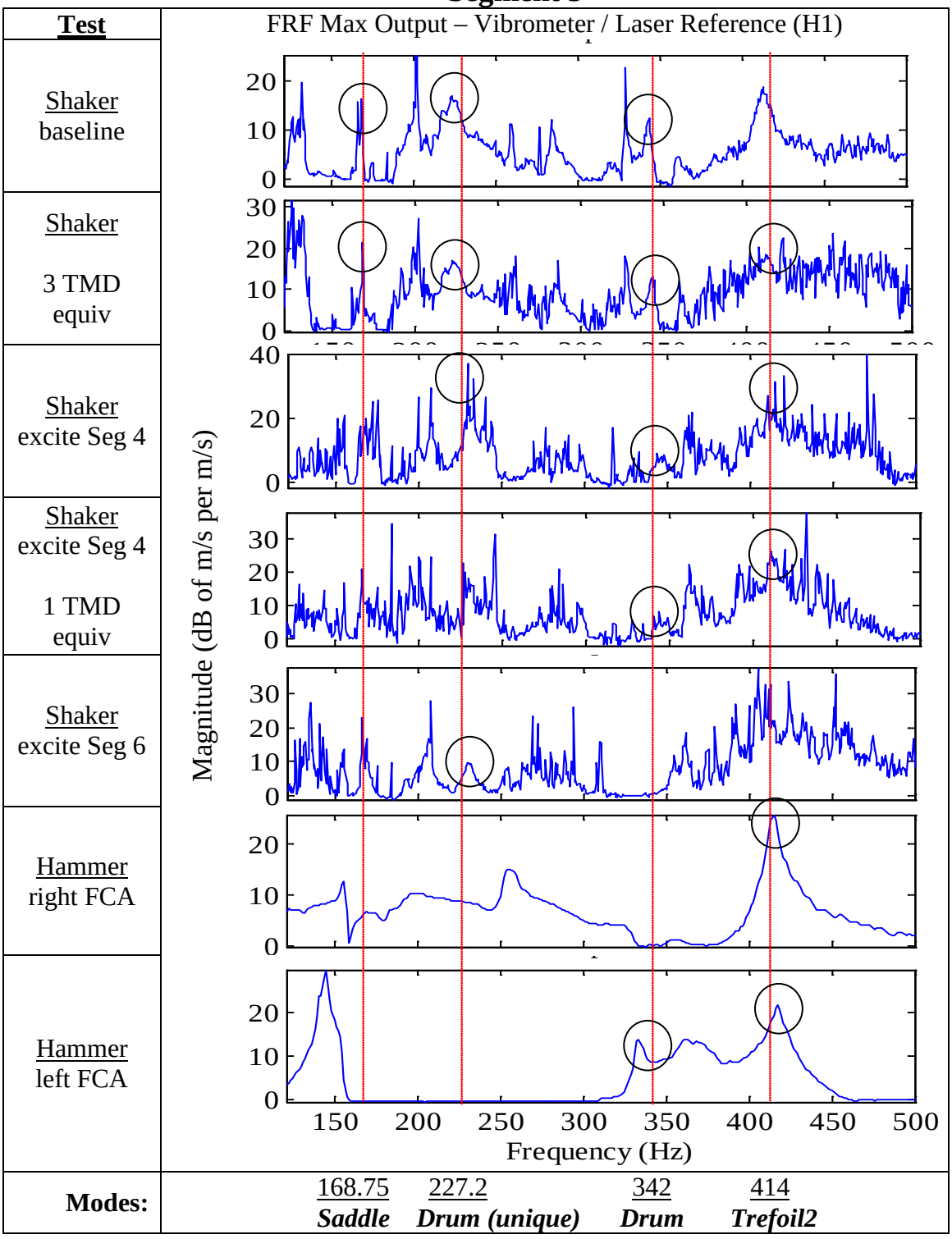

Figure 30. Segment 5 FRFs (121 – 500 Hz)

Segment 5

FEM	*Shaker: baseline*	*Shaker: 3 TMD equiv*	*Shaker: excite 4*	*Shaker: excite 4 1 TMD equiv*	*Shaker: excite 6*	*Hammer: right FCA*	*Hammer: left FCA*
Saddle							
157.8154	168.75	168.75					
Drum (unique)							
	223.75	223.75	230.0		231.25		
Drum							
279.8305	343.125	343.75	344.3761	344.3761			333.75
Trefoil2							
379.8146		412.5	413.751	411.25		415.0	417.5

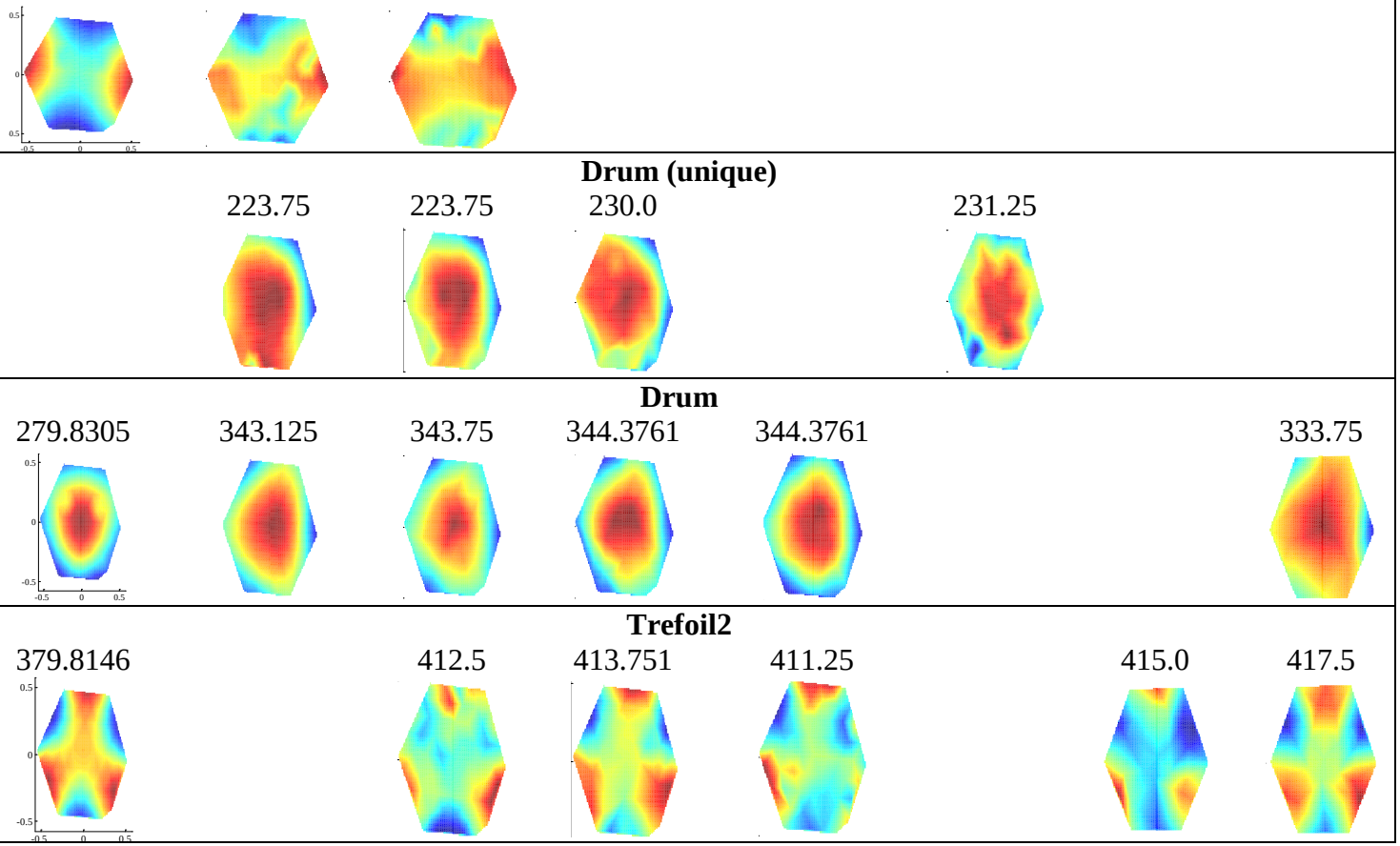

Figure 31. Segment 5 experimental mode shapes with FEM comparison

Modal Testing – Segment 6 Results

Modal testing of segment 6 produced high quality data with resonances at the four expected modes occurring in almost all shaker and hammer runs. As shown in Figure 32, the segment 6 saddle mode resonated near 161 Hz similar to the 162.5 Hz found during previous testing. The drum mode was found near 316 Hz, trefoil1 mode near 345 Hz, and trefoil2 mode near 423 Hz. Figure 33 presents the mode shape contours at the frequencies highlighted by the black circles on the FRF plots. Modal damping was estimated to be a maximum of 0.4%, occurring at the saddle and drum modes.

Modal Testing Summary

Based upon findings from modal testing, Table 8 summarizes the high frequency segment bending modes that were excited consistently and with distinct mode shapes. The results in this table were used as the basis to begin model tuning efforts and model-to-experiment comparisons described in the next section.

Table 8. SMT experimental natural frequencies (Hz, segment bending modes)

Mode	**segment 4**	**segment 5**	**segment 6**
Saddle	151	159	161
Drum		227	
Drum	323	344	315
Trefoil1	278		345
Trefoil2	406	415	423

Segment 6

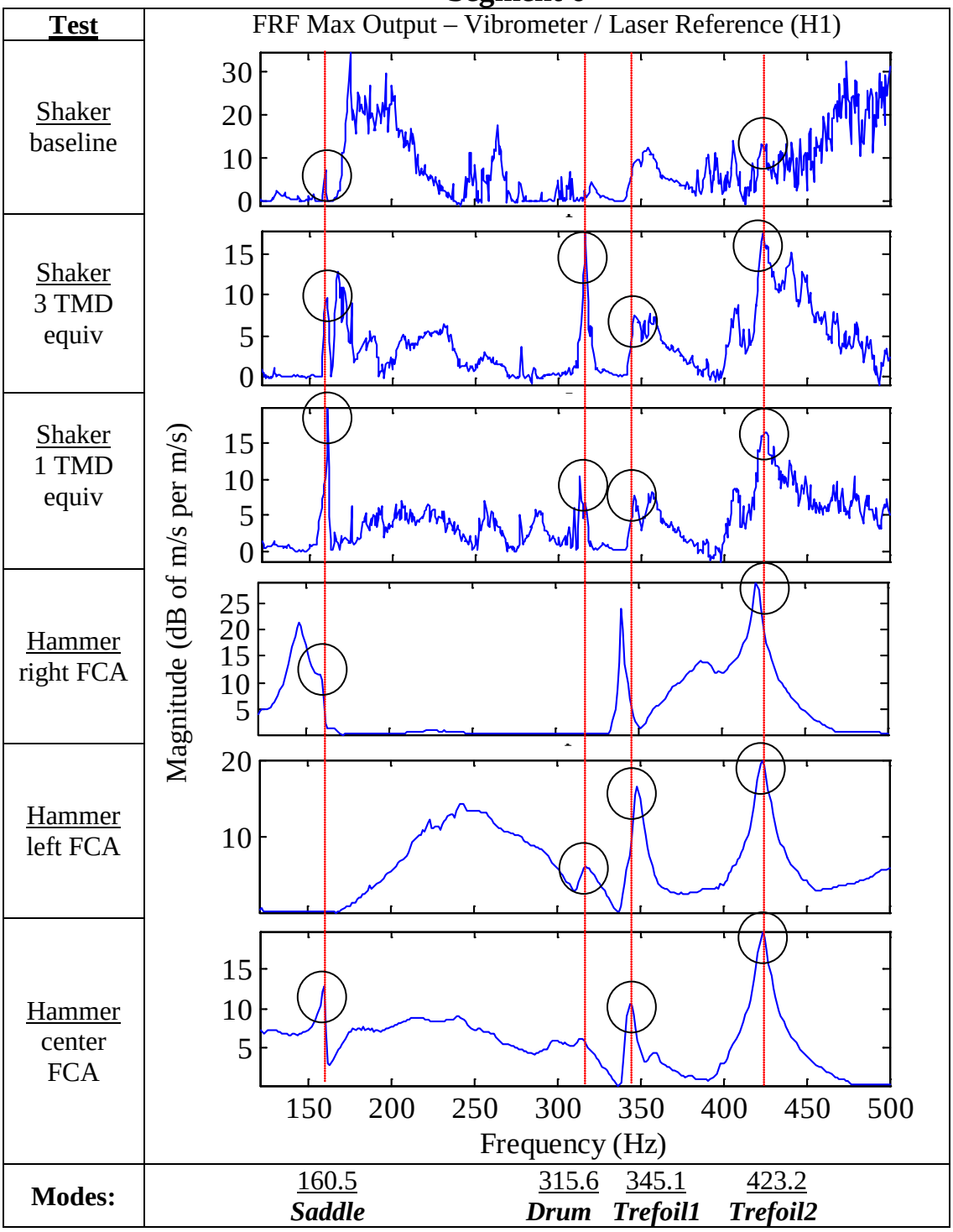

Figure 32. Segment 6 FRFs (121 – 500 Hz)

Segment 6

FEM	*Shaker: baseline*	*Shaker: 3 TMD equiv*	*Shaker: 1 TMD equiv*	*Hammer: right FCA*	*Hammer: left FCA*	*Hammer: center FCA*
Saddle						
157.6187	160.6274	160.6274	161.25	160.0		160.0
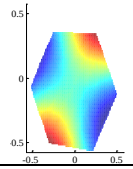	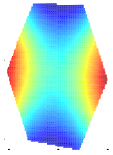	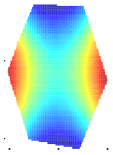	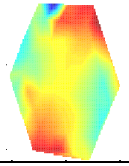	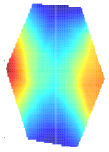		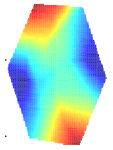
Drum						
303.9119		316.875	313.75		316.2549	
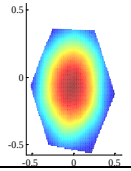		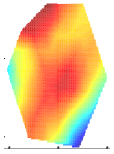	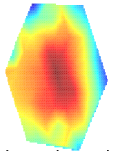		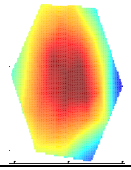	
Trefoil1						
330.1396		346.875	346.2511	340.0	348.75	343.75
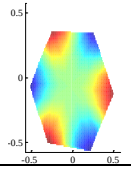		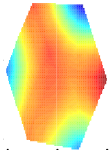	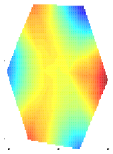	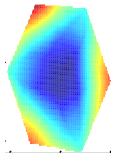	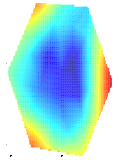	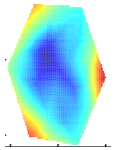
Trefoil2						
383.8003	423.75	423.75	423.1259	421.2537	423.75	423.75
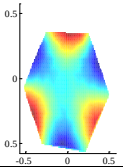	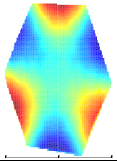	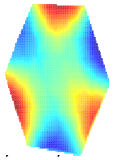	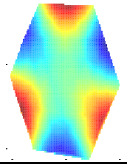	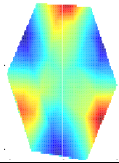	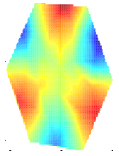	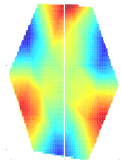

Figure 33. Segment 6 experimental mode shapes with FEM comparison

Model Tuning and Prediction

The 25 run FCD with analysis results are provided in Appendix C. The first local segment bending mode of segments 4, 5, and 6 were used to compute objective function J values. A 2nd-order polynomial equation was fit from results of the 25 runs and values for the four design variables (E) were predicted to minimize the J value. A validation run was performed using the values shown in Table 9.

Table 9. Design variable values predicted to minimize objective function

	Coded Units				Natural Units (Young's Modulus, E)			
Segment	X1	X2	X3	X4	Layer1 Inner	Layer1 Outer	Layer2 Inner	Layer2 Outer
4	0	0	-0.242	0.02	3549800	4319700	842517	1133730
5	0	0	0.198	-0.2	3549800	4319700	1331577	889200
6	0	0	0.0835	0.2	3549800	4319700	1204310	1333800

The error between the experimental and FEM frequencies are shown in Table 10. Cells highlighted orange show increased modeling error compared to the original HiFi-FEM. The tuned ROSE-FEM had a maximum error increase of 3.1%, for segment 4 trefoil1 mode. Basic tuning to the first segment modes proved to yield very good results with error across seven of the eleven modes decreasing and the remaining four modes being near the baseline model (maximum increase of 2.1% error on the segment 4 drum mode).

Table 10. Percent error between experimental and FEM frequencies

			% Error			
Mode	Segment	Freq (Hz)	Original HiFi-FEM	Baseline ROSE-FEM	Tuned ROSE-FEM	**% Improvement**
Saddle	4	151	4.83%	-4.35%	-1.47%	3.36%
	5	159	9.6%	0.7%	1.6%	8.02%
	6	161	5.6%	2.1%	-0.4%	5.14%
Drum	5	227	not predicted			
	4	323	20.5%	7.1%	9.2%	11.34%
	5	344	21.7%	18.7%	16.5%	5.18%
	6	315	14.1%	3.5%	2.9%	11.20%
Trefoil1	4	278	-13.3%	-18.8%	-16.4%	-3.08%
	6	345	8.2%	4.3%	1.0%	7.17%
Trefoil2	4	406	5.5%	5.6%	7.3%	-1.83%
	5	415	8.1%	8.5%	9.3%	-1.21%
	6	423	8.9%	9.3%	6.7%	2.15%

A direct comparison of experimental frequencies to FEM eigenvalues is shown in Figure 34. Corresponding modes from each FEM model lie on a horizontal line, with three examples highlighted with grey ovals. The goal of tuning using a frequency-based objective function is to have the tuned model modes lie on the “exact fit” line. A second plot focusing only on the saddle mode is shown in Figure 35. As can be seen, the initial tuning approach yielded positive results in achieving a more accurate FEM, but additional tuning is suggested to further decrease the error seen in the segment 5 drum and segment 4 trefoil1 modes. Less than 2% error exists in the initial tuned ROSE-FEM for modes less than 200 Hz. For modes greater than 200 Hz, up to 16.5% error still exists, driving higher uncertainty for the drum, trefoil1, and trefoil2 modes.

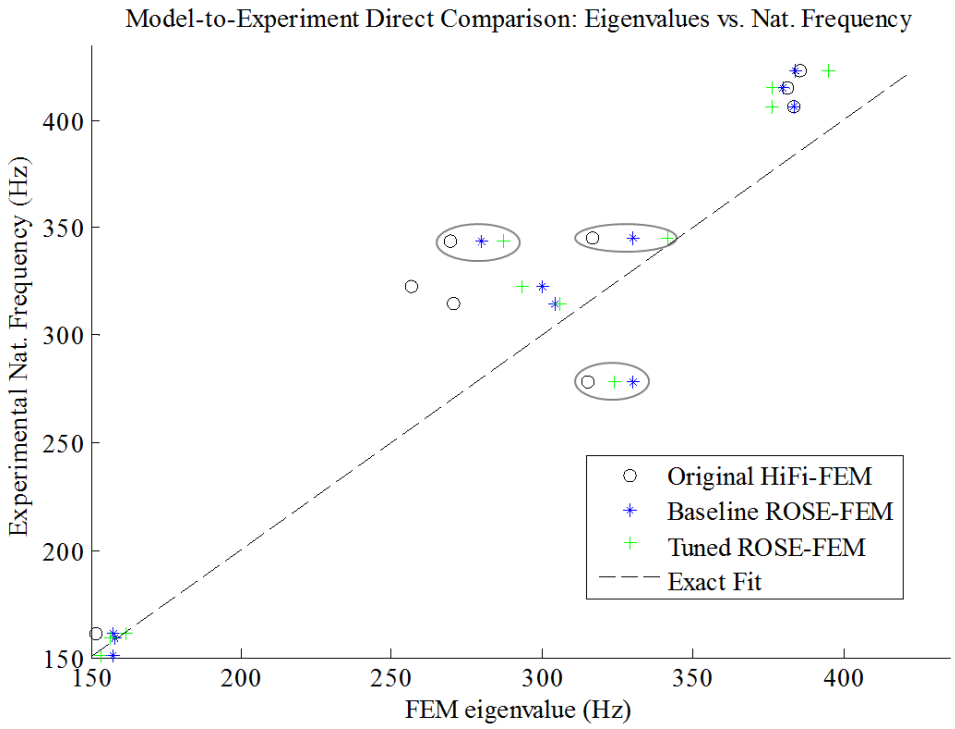

Figure 34. Frequency direct comparison plot (all high frequency bending modes)

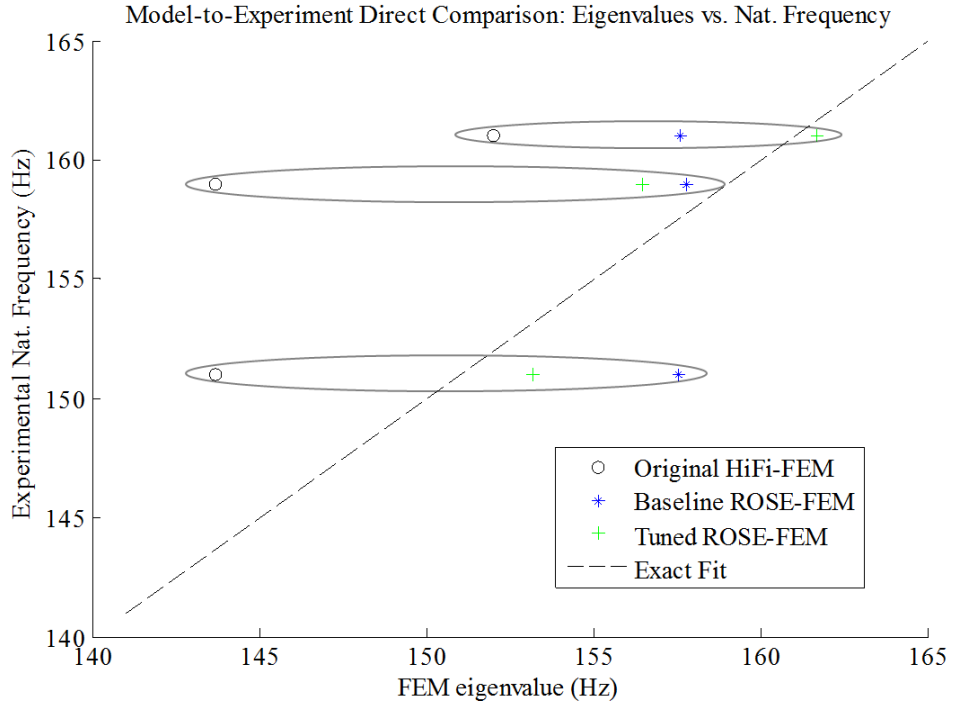

Figure 35. Frequency direct comparison plot (saddle mode)

V. Discussion

Conclusions

Substantial gains in segmented mirror telescope FEM efficiency were obtained by implementing the superelement technique while also targeting the mirror segments as a prospective region for reduction in model complexity. Traditionally, analysis of large FEMs, such as represented by the high-fidelity (HiFi)-FEM in this thesis, would progress by obtaining an analytical solution for only a particular substructure of interest. However, the model is often extremely sensitive to the assumed boundary conditions. In addition, all dynamic behavior due to substructure interfaces will be left unaccounted for. Due to symmetry in the primary mirror of segmented optics systems, using the methods presented in this thesis, a multimillion degree of freedom FEM can be reduced to a size approximated by Equation (7).

$$\text{ROSE-FEM size} \approx elem_{residual} - n_{segment} \times elem_{segment} \times 96\% \qquad (7)$$

In this equation, $elem_{residual}$ is the number of elements (or nodes) representing the region where analytical predictions are desired, such as the primary mirror, $n_{segment}$ is the number of segments, and $elem_{segment}$ is the number of elements (or nodes) in an individual segment. For example, the JWST 's "dynamics are represented by a state-space model, which is constructed using the mass-normalized eigenvalues of the observatory finite element model" (Meza, Tung, Anandakrishnan, Spector, & Hyde, 2005, p. 13) with approximately 30 million degrees of freedom. With 130 thousand elements per segment (Genberg, Bisson, Michels, & Doyle, 2006), a reduced-order superelement (ROSE)-FEM

of the JWST would be expected to have between 94 and 245 thousand elements (92-98% reduction in model size).

Specifically for the HiFi-FEM (622 thousand elements) of the Segmented Mirror Telescope testbed at the Naval Postgraduate School, nearly 50% of the model elements were replaced by four superelements and the remaining residual structure was reduced by over 84% leaving a model with 48 thousand elements. A FEM at less than 1/12 the original size can be analyzed far more efficiently. Eigenanalysis using the ROSE-FEM, for the first 120 modes, average under eight minutes using a US Air Force standard equipped desktop (dual processor, 4 GB RAM) requiring 4 GB of temporary hard drive space. Equivalent analysis using the HiFi-FEM requires over two hours (16 processors, 64 GB RAM clustered server) and 160 GB of temporary drive space.

Remarkably, the drastic decrease in model size is accompanied with negligible loss in accuracy of the FEA. Prior to tuning the ROSE-FEM, a direct comparison of high frequency modes shows the reduced model closely matched or improved upon the HiFi-FEM, relative to experimental results from modal testing, for three of the four dominate segment modes.

After performing 25 eigenanalysis runs for a simple characterization of the ROSE-FEM's dynamic response, the model was tuned and error (comparing the difference between the modeled and experimental natural frequencies greater than 100 Hz) was reduced to 6.7% on average (HiFi-FEM at 11%).

In summary, the research detailed in this thesis validated FEA modeling techniques with experimental data to allow effective and efficient prediction of the dynamic behavior of complex systems with isogrid structure.

Future Work

An efficient FEM of the SMT has been developed, setting the stage for iterative model tuning approaches. However, extensive efforts into acquiring a robust, fully tuned model were not accomplished. While initial model-to-experimental data comparisons were made based upon natural frequencies, mode shape comparisons were only performed qualitatively with contour and three-dimensional surface plots.

Formal metrics to compare analytical and measured mode shapes have been developed, such as Modal Scale Factors and Modal Assurance Criterion, and are important to the validation of a FEM (Marwala, 2010). Use of an objective function based upon both mode frequencies and shapes would ensure an effective state-space model to control external disturbances causing mirror surface figure degradation. In addition, other response surface methodologies developed specifically for deterministic computer models are recommended. Space filling designs place no assumption on the complexity of the response surface (FCD implemented assumes 2^{nd}-order model). These designs, analyzed using a Kriging/Gaussian interpolative method, are ideal for tuning the deterministic model to experimental data collected from the physical system.

It is recommended that further efforts to validate the SMT FEM should be conducted by a researcher with sufficient knowledge of optimization processes and response surface methodology, control theory, and a background in FEA. An understanding of the development of optical line-of-sight model would be beneficial as well. The research detailed in this thesis developed the initial groundwork to enable the proposed multidisciplinary approach required to demonstrate high-resolution imaging capability with a space-based segmented mirror telescope.

Appendices

Appendix A. FEM Superelement Interface (Master) Nodes (A-Set)

64 nodes

(SEID – superelement identifier)

The following nodes define the partitioning of the HiFi-FEM into superelements.

SEID 1 (42 nodes)

Petals to Central Support (24)	Petals to Primary Mirros (FCAs, 18)
1980004	8151128
1980001	8151142
1980002	8151114
1980003	8251128
1980033	8251142
1980032	8251114
1111433	8351128
1112867	8351142
1121433	8351114
1122867	8451128
1131433	8451142
1132867	8451114
1141433	8551128
1142867	8551142
1151433	8551114
1152867	8651128
1161433	8651142
1162867	8651114
6432002	
6432001	
6434002	
6434001	
6436002	
6436001	

SEID 2 (12 nodes)

Tower to Central Support(6):	Tower to Secondary Mirror (6):
1980007	3608007
1980005	3608008
1980006	3608009
1980035	3608010
1980034	3608012
1980036	3608011

SEID 3 (4 nodes)	SEID 4 (6 nodes)
Base Systems to Central Support (4):	Isolator Rods to Central Support (6):
1980012	1980020
1980011	1980021
1980043	1980052
1980044	1980051
	1980054

Appendix B. Conference Manuscript

Model Complexity Reduction of a Segmented Mirror Telescope

Luke C. Dras [1], Alan L. Jennings [2], and Richard G. Cobb [3]
Air Force Institute of Technology, WPAFB, OH, 45433

Segmented mirror telescopes enable large apertures to be formed from smaller mirror segments. The supporting structures generally involve complex hardware so finite element models are used to predict how the equipment will behave under different environmental conditions. This paper takes a very complex high fidelity finite element model, partitions its substructures into superelements, and reduces the number of elements while matching the structure's dynamic characteristics. It is then possible to tune the reduced-order model based on measured vibration data. The methodology matches specific components, such as the mirrors, and then verifies that the overall structure has the same behavior as the full order model. Results demonstrate how common structures, such as an isogrid, can be modeled by equivalent plate elements and preserve the dynamic characteristics from the measured vibration data.

Nomenclature

dof	= degree of freedom
EOM	= equation of motion
FEM	= finite element model
HiFi-FEM	= high fidelity finite element model
Hz	= Hertz
RO-mirror	= reduced-order mirror segment
ROSE-FEM	= reduced-order, superelement finite element model
SEID	= superelement identification
SMT	= segmented mirror telescope
TMD	= tuned mass damper

I. Introduction

Atmospheric optics have reached unprecedented accomplishments in resolution. Adaptive optic techniques are able attenuate image jitter and remove atmospheric distortion effect by deforming a mirror to compensate.[1] Different thermal, density, and wind conditions can cause the light to bend or arrive out of phase. The difference in arrival phase is termed wavefront error and can be measured using wavefront sensors.[2] In addition, various disturbance sources can interact with the dynamic characteristics of the optical system causing significant image degradation jitter. The wavefront sensor and dynamic sensors can be used in a feedback control system.[3] For further increases in resolution, the Rayleigh criterion dictates large aperture optics are needed. Large monolithic mirrors, particularly for space-based systems, can be problematic for telescopes due to weight, manufacturability, and portability. The solution is to use lightweight mirror segments which can be assembled into an array to effectively form a single large mirror.[4]

As the position of each mirror segment can be individually adjusted, alignment can be corrected with precision actuators. However, each mirror can vibrate independently. Some vibration can be compensated for by feedback with adaptive optic techniques. The amount of correction is limited, so the bound of aberration caused by vibration needs to be known. In addition, the aberration should be known a priori so the performance of the system can be predicted prior to investing in construction and deployment of the telescope.

[1] Captain, M.S. Student, Department of Aeronautics and Astronautics, 2950 Hobson Way, Student AIAA Member.
[2] Research Assistant Professor, Department of Aeronautics and Astronautics, 2950 Hobson Way, AIAA Member.
[3] Associate Professor, Department of Aeronautics and Astronautics, 2950 Hobson Way, AIAA Associate Fellow.

Optical performance due to vibration can be predicted from finite element analysis and verified with system modal testing. Finite element models can be used to find the system's dynamic characteristics.[5, 6] Design iteration can be used to move all natural frequencies higher than a set limit, and finite element analysis offers a cost effective tool for design iteration. The model should be tuned and validated by test data, which requires iterating over model parameters.

This paper demonstrates creating a reduced-order model for a space-based segmented mirror telescope (SMT). For the current application, a high fidelity finite element model is available, but the large number of degrees of freedom make it cumbersome for use in the tuning process. The process for creating a reduced-order model is first presented and then comparisons to the high fidelity model are provided. A description of the high fidelity model and reduced-order modeling details are given in Section II. Section III describes the equipment and modal testing procedure used to obtain dynamic characteristics of a segmented mirror telescope. Comparison of the reduced-order model to the high fidelity model, as well as the experimental data collected, is discussed in Section IV. The paper concludes in Section V. with a summary of the results and recommendations.

Segmented Mirror Telescope

The segmented mirror testbed is a laboratory deployable, lightweight optical telescope. The telescope serves as an experimental testbed used to demonstrate adaptive optic and other telescope imaging technologies. Though it contains state of the art technology and lightweight construction, the telescope was only intended as a research and development testbed. Housed at the Naval Postgraduate School's (NPS) Segment Mirror Telescope laboratory, it is mounted on an isolation table within an internal structure to help isolate it from stray light or seismic and wind disturbances.[7]

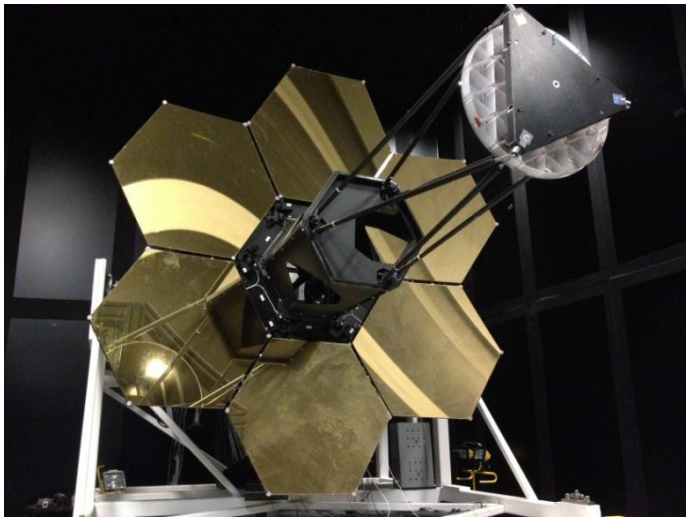

Figure 1. 3 meter Cassegrain reflector with primary mirror formed from 6 mirror segments.

The basic configuration is that of the Cassegrain reflector with a large concave primary mirror and smaller secondary mirror mounted on a tower, see Figure 1.[8] Located behind the primary mirror are additional sensors such as Shack-Hartmann wavefront sensors, and adaptive optics devices such as a fast steering mirror for global tip and tilt motions. The primary mirror is composed of 6 hexagonal mirror segments that each have 6 coarse and 3 fine position actuators and 156 face-sheet actuators.[9] The width of the combined mirror is 3 m with each mirror being 1 m wide. Each mirror has a triangular isogrid upon which the face sheet actuators are mounted.

II. Finite Element Model

Tuning a finite element model (FEM) requires an iterative process to minimize a cost/objective function, often by means of constrained optimization or gradient-based approaches. The cost function is developed as a function of modal characteristics (eigenvalues and eigenvectors) and represents the correlation between simulated predictions and system data extracted through experimentation. Multiple simulations must be performed while incrementally adjusting FEM design variables such as material Modulus of Elasticity and/or mass density properties. As these optimization approaches can require many iterations a high fidelity finite element model (HiFi-FEM) is not desirable for tuning purposes. A reduced-order model that adequately approximates low-order dynamic characteristics is therefore preferred.

The process implemented to tune the FEM of the SMT can be broken down into three fundamental efforts. First, creation of a reduced-order substructured (superelement) model (ROSE-FEM) for predicting eigenvalues and eigenvectors. Then modal testing of the SMT must be performed to obtain natural frequencies, mode shapes, and an estimate of system damping. Finally key parameters of the ROSE-FEM must be identified and adjusted iteratively to minimize model error. Upon completion of these efforts, frequency dependent model uncertainty factors can be generated to assess applicability of the model.

A. High Fidelity Model

Finite element models are used to capture deflections and dynamics of complex structures by approximating them with a set of interrelated small linear elements. All analysis done in this work is linear, as justified by the small amplitude displacements when in operation. By considering the mass distribution and the relative stiffness of adjacent nodes, the vibration mode shapes can be determined. The system for linear dynamics is

$$[\mathrm{M}]\ddot{\bar{x}} + [\mathrm{C}]\dot{\bar{x}} + [\mathrm{K}]\bar{x} = \vec{F} \tag{1}$$

with x being the amplitude of each degree of freedom (dof) of the model, M as the inertial matrix, C as the damping matrix, K as the stiffness matrix, and F used for a forcing excitation. The eigenvalue of K in the space of M give the mode shapes with the eigenvalue used to calculate the vibration frequency. Many programs exist that handle the numeric challenges of solving for eigenvectors of large systems.

A NASTRAN compatible model was provided by NPS. First attempts at model validation are presented in Ref. 10. The model consists of the full telescope structure to where it mounts to the adapter ring of the base, as shown in Figure 2. It includes mass and spring elements in addition to the structural elements. The spatial resolution is very high resulting in 2.63 million degrees of freedom. The solver ran on a Linux cluster for large memory allowances and typically required about 140 minutes for batches of 10 modes. Even simple operations like model rendering were cumbersome, causing concern for planned iterative model tuning schemes. To meet the primary objective of creating a more efficient segmented mirror telescope finite element model, model substructuring and the use of fewer elements in key components was implemented.

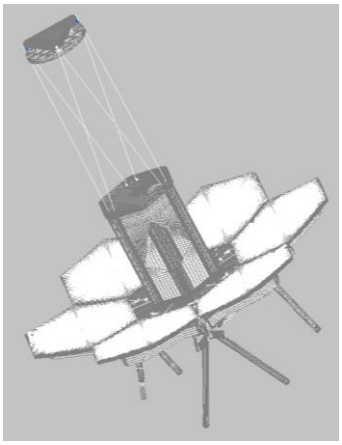

Figure 2. High fidelity finite element model.

B. Superelement Partitioned Model

The use of the external superelement technique for analyzing large finite element models is frequently implemented to both reduce simulation run times as well as allow simulations be performed with limited computer memory. FEM superelement order reduction techniques are described in detail in Ref. 11 and can be used in analysis of both static and dynamic simulations.

External superelements represent groups of finite elements within the model which are condensed into a single element, analyzed independently, and assembled into a reduced model for subsequent simulations. Each substructure of the system being represented by the 2nd-order equation of motion (EOM) shown in equation (2)

$$[\mathrm{M}]\{\ddot{x}\} + [\mathrm{C}]\{\dot{x}\} + [\mathrm{K}]\{x\} = \{F\} \tag{1}$$

with matrices sized according to the dof in the substructure. By partitioning each substructure EOM by internal slave (s) and boundary master (m) dof a partitioned substructure can be written as

$$\begin{bmatrix} \mathrm{M}_{mm} & \mathrm{M}_{ms} \\ \mathrm{M}_{ms}{}^{T} & \mathrm{M}_{ss} \end{bmatrix} \begin{Bmatrix} \ddot{\bar{x}}_m \\ \ddot{\bar{x}}_s \end{Bmatrix} + \begin{bmatrix} \mathrm{C}_{mm} & \mathrm{C}_{ms} \\ \mathrm{C}_{ms}{}^{T} & \mathrm{C}_{ss} \end{bmatrix} \begin{Bmatrix} \dot{\bar{x}}_m \\ \dot{\bar{x}}_s \end{Bmatrix} + \begin{bmatrix} \mathrm{K}_{mm} & \mathrm{K}_{ms} \\ \mathrm{K}_{ms}{}^{T} & \mathrm{K}_{ss} \end{bmatrix} \begin{Bmatrix} \bar{x}_m \\ \bar{x}_s \end{Bmatrix} = \begin{Bmatrix} {}^{\mathrm{I}}\mathrm{F}_m \\ 0 \end{Bmatrix} + \begin{Bmatrix} {}^{\mathrm{E}}\mathrm{F}_m \\ 0 \end{Bmatrix}. \tag{2}$$

Master nodes represent connection points between superelements and the remaining structure, as well as locations of constraints and externally applied forces ($^{\mathrm{E}}\mathrm{F}_m$). Dynamic Condensation (also known as Component Modal Synthesis) is recommended when conducting dynamic analysis as the eigen solution of the resulting reduced model exactly replicates dynamics of the full model.[11] During condensation, internal displacements within the superelements are translated to the master nodes through internal forces $^{\mathrm{I}}\mathrm{F}_m$. Degrees of freedom associated with the superelements can

then be removed from the model leaving the residual structure to be analyzed independently. Regions of interest, such as the mirror segments, must remain as residual structure. The reduced model can then be written as

$$[M_R]\ddot{\vec{x}}_m + [C_R]\dot{\vec{x}}_m + [K_R]\vec{x}_m = \left\{ {}^{I}F_m \right\} + \left\{ {}^{E}F_m \right\}. \quad (3)$$

In application to the SMT, knowledge of the dynamic behavior of the primary mirror to disturbance is essential to creation of a control system to reduce or eliminate image jitter and wavefront error. Therefore the six primary mirror segments are classified as residual structure. A diagram depicting the FEM partitioning into single-level superelements is shown in Figure 3. The secondary mirror and central hexagon segment support structure are also included as residual structure. The secondary mirror is included as a region of interest as it was shown in early system testing that the tower supporting this mirror is susceptible to large amplitude motion during low frequency disturbances. The central segment support structure was found to be a critical interface between the primary mirror segments and the remaining structure. Including the central support as residual structure simplifies partitioning the remaining structure into superelements. A graphical view of the superelement partitioned FEM is shown in Figure 4.

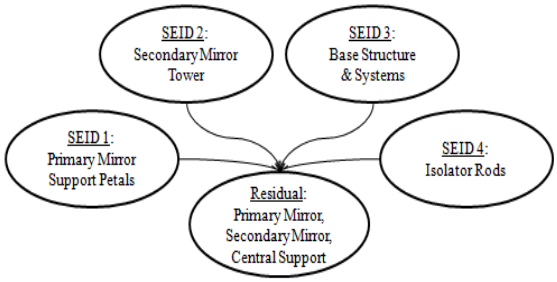

Figure 3. SMT FEM Single-Level Substructuring

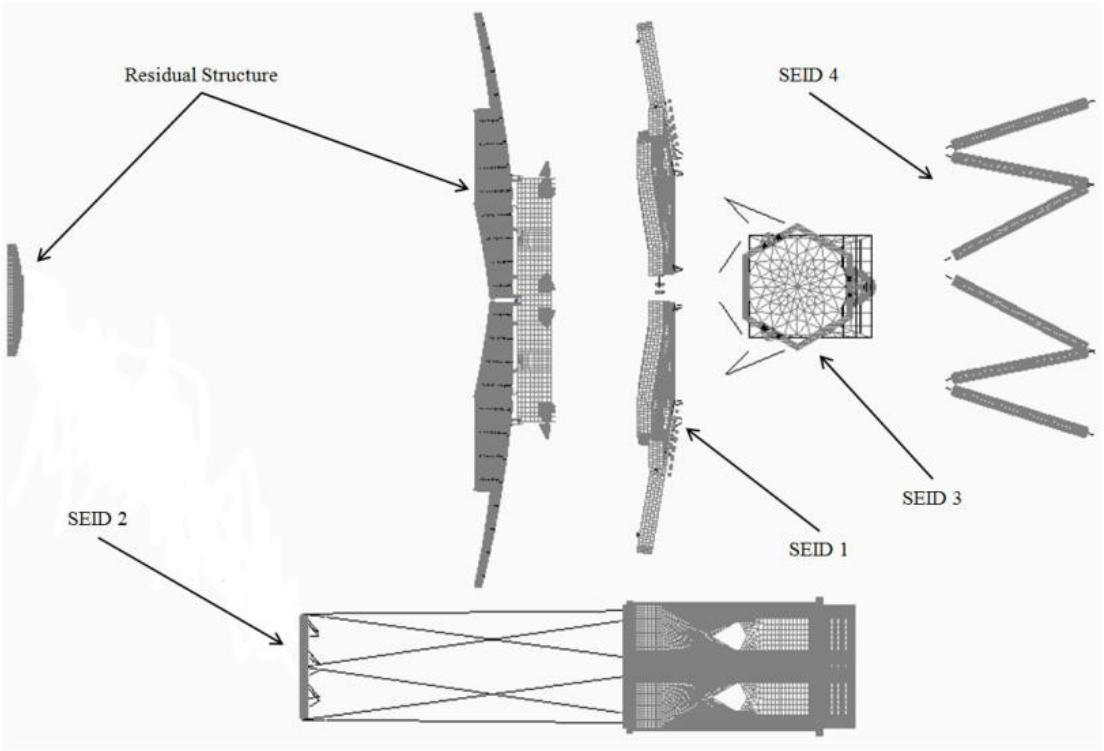

Figure 4. SMT FEM Substructuring Scheme

The residual (region of interest) structure includes the six primary mirror segments (with the face-sheet actuators for wavefront error control), the secondary mirror, and the central hexagon segment support structure. Superelement 1 (SEID1) consists of the segment support petals, including the hexapods and flexures with allow coarse and fine control of the primary mirror segments. The secondary mirror support tower is defined by Superelement 2 (SEID2).

Superelement 3 (SEID3) includes all components and sensors in the optical drive train following the secondary mirror and supporting structure. Lastly, Superelement 4 (SEID4) defines the isolator rods that ground the SMT.

To perform FEM dynamic simulations, a single eigenanalysis run is performed on each superelement independently, requiring on average less than 4 minutes per superelement using a standard equipped computer (2.7 GHz dual processor, 4GB RAM). Then, iterative simulations need only be performed on the residual structure (320 thousand elements, 1.49 million dof).

C. Reduced-Order Mirror Segments

Beyond partitioning the HiFi-FEM into superelements, further improvements in simulation efficiency is possible by reducing the complexity of the residual structure. With over 40% of the nodes/elements of the HiFi-FEM being used for modeling the six hexagonal mirror segments, large gains in simulation run times are possible with minor loss in the accuracy of simulation results.

A single mirror was separated for comparison to verify that a reduced-order mirror segment (RO-mirror) model is functionally equivalent to the high fidelity mirror segment model. Equivalence was determined in static and dynamic senses.

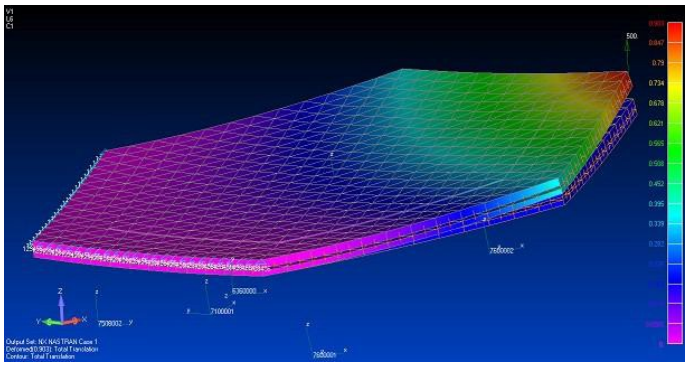

Figure 5. Static equivalence, two edges of the mirror were fixed with a load applied to the opposite corner.

Static equivalence is based on constraining two edges of a mirror and applying a static load on the opposite corner, as shown in Figure 5. Displacements across the surface were compared. This test demonstrated that the RO-mirror had the same stiffness as the high fidelity model as the load produces the same deflection on each.

Dynamic equivalence is shown by a normal modes analysis, which computes the stiffness matrix in the space of the mass matrix. The three mirror supports joints were fixed, shown in Figure 6. These results can aid in tuning the model to experimental data, and for a line-of-sight model using geometric optics. The first ten modes were used for comparison.

The mirror segments in the HiFi-FEM involve a complex structure modeled with plate, laminar plate, bars, solids, and rigid elements. As seen in Figure 7, the plate elements composed a structural isogrid mirror substrate. The coarse isogrid is used for adaptive optics with a notch replaced with a bar representing the face-sheet-actuators. The fine isogrid has a deeper well around the outer edge with the rest having shorter walls. The mirror surface was comprised of laminar plate elements, including the primary material and two thin coating layers. Attachment points of the supports were modeled with bar, solid, rigid, and spring elements.

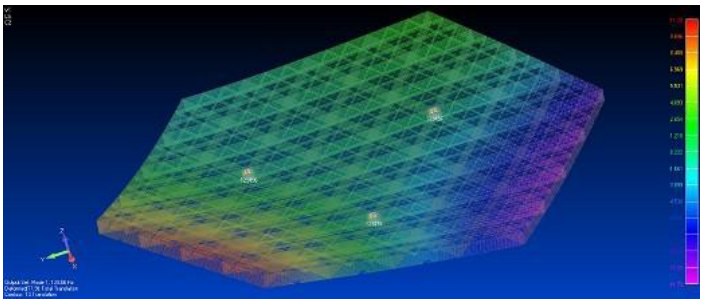

Figure 6. Dynamic equivalence, three mirror support joints were fixed.

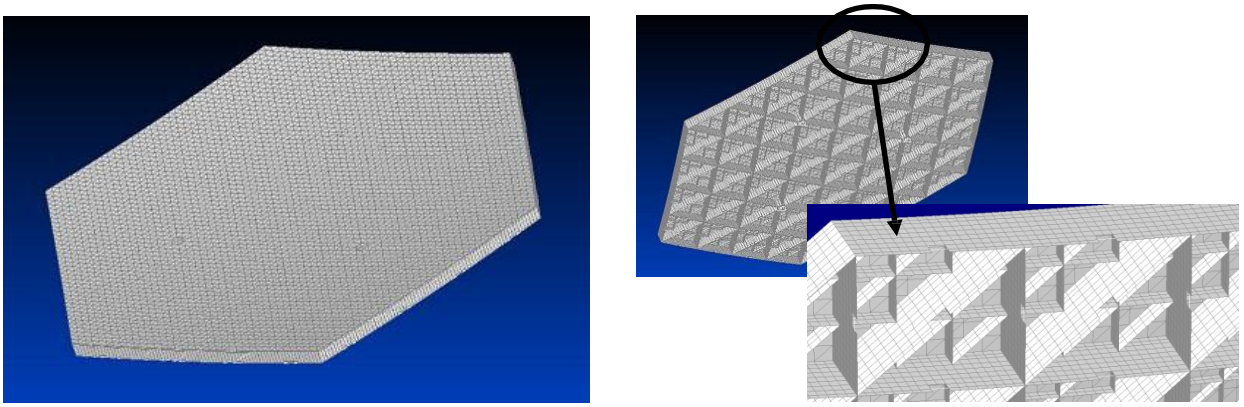

(a) Face (b) Back

(c) Isogrid detail and support joint

Figure 7. HiFi-FEM mirror model laminate face with isogrid back and support joints.

To reduce the complexity of the mirror, a common modeling technique is to model uniform honeycomb structured panels with a single flat plate and adjust the material Modulus of Elasticity (E) and thickness (t) with equivalent values (E* and t*).[12,13] This method, originally developed by NASA in 1973, was established to allow for more efficient load analysis of geometrically complex panels/plates.[14]

This technique can be applied to isogrid panels using appropriate geometric parameters. To accommodate the nonuniform isogrid panel of the SMT mirror a two-layer plate model was developed, as shown in Figure 8. There were three unique web depths modeled by a different number of equally sized elements: 2 elements for the inner, fine isogrid; 3 elements for the outer, fine isogrid; and 9 elements for the coarse isogrid. The first "base" plate layer models the mirror surface and base isogrid depths (6 units high along outer edges, 7 units high on interior). The second plate layer models the section of the coarse isogrid, but only the web depth not accounted for in the base layer (3 units deep along outer edges, 2 units deep on interior). To model this nonuniform isogrid, the layers are meshed with separate material properties (E* and t*) for the outer versus the inner plate elements. To ensure accuracy of rotational inertia properties, the second layer is offset from the base layer but tied to it via rigid links. See Figure 8 for a pictorial view of the construction of the RO-mirror. The inner plate elements are hidden for clarity.

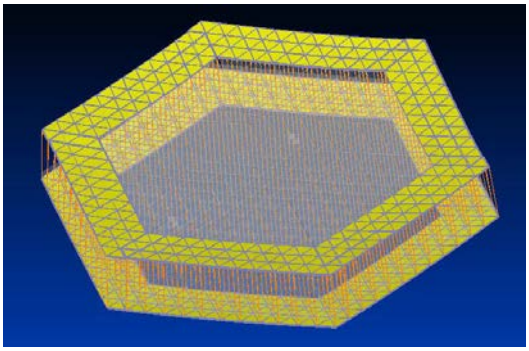

Figure 8. RO-mirror two-layer plate model

The density was initially calculated based on the volume replaced by the equivalent plate with the offset of the plate based on the center of the section being replaced. This preserved not only the absolute mass, but the center of gravity also. The global moments of inertia were also compared, agreeing within 5%.

Twelve parabolic triangular plate elements were used along each outside edge. This element sizing matches the isogrid sizing

in order to ensure the RO-mirror has resolution equal to the measurements and can easily connect to the full telescope model. This mesh resolution was fine enough that effects due to the concavity of the mirror can be seen in modal analysis.

The solid, bar, and rigid elements of the connection points seen in Figure 7-C were replaced with a point mass element with a mass equivalent to the removed elements. Comparison of the RO-mirror to the high fidelity mirror is presented in section IV.

III. Vibration Data

A. Testing Environment

The SMT is located on an ≈3 m × 3 m pneumatic isolation table with an ≈1 m × 8 m extension to allow test equipment to be placed on the table. The isolators are tuned for seismic disturbances of frequencies below 10 Hz. The SMT is also housed in a dark tent to isolate the telescope from stray light, air currents or dust and other debris.

However, the closed volume is prone to internal acoustic waves. The enclosure is created from metal panels, similar to ductwork but painted black, and supported by a steel truss structure. With its length of 16 m, the first three acoustic modes of the enclosure are at 11, 21 and 32 Hz.[15] The segmented mirror is positioned roughly a third of the distance from the end, so each has significant amplitude at the distance of the primary mirror. For modal testing, a scanning laser vibrometer was mounted on the isolation table between 2 to 7 m from the primary mirror segments. Measurements were taken across the primary mirror near the intersections of the isogrid. A true mirror would ideally reflect opposite the source direction, but the mirror had a sufficiently diffuse surface so enough signal return was obtained for taking measurements directly on the mirror. These locations are shown in Figure 9.

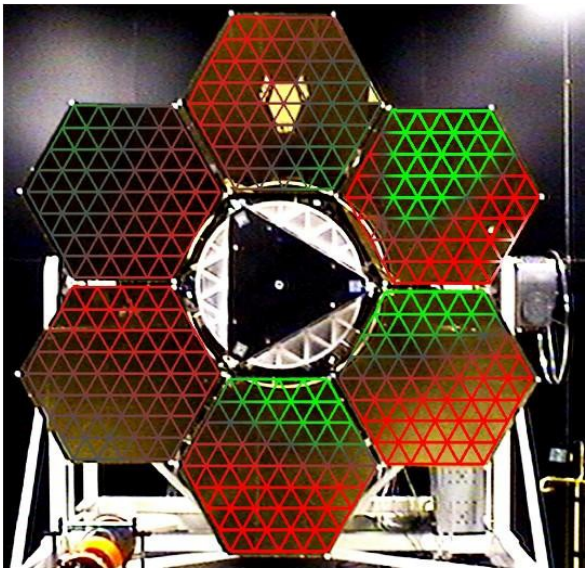

Figure 9. Measurements were taken across the mirror near the isogrid intersection locations.

B. Laser Vibrometry

Results from initial 2011 SMT vibration tests have been presented in Ref 10. Laser vibrometry is based on the Doppler principle. As light reflects off a moving surface, the frequency is shifted. By comparing the frequency shift to the original beam, the difference can be measured. Direction towards or away is determined by applying a known frequency shift in addition to the shift due to motion. Note that by measuring the frequency shift, rather than intensity, results are indifferent to distance to the surface or its emissivity. Vibrations on the order of 10 nm/sec can be measured despite taking the measurement from meters away. Due to the high frequency of the laser, the bandwidth of the response is primarily limited by the analog to digital sample rate. At every measurement location, the laser dwells to determine the vibration of the point. By measuring the vibration with respect to a reference signal, the relative amplitude and phase between measurement points can be determined. Taking all the measurements, the operation deflection shape can be determined and checked for consistency against the structural modes of the test article. For the initial tests, data was collected via ambient testing where acoustic waves primarily excited the structure.

A Polytec PSV 400-3D scanning vibrometer was used with an OFV-5000 controller. This vibrometer uses an eye-safe red laser. The reference signals was provided by another laser vibrometer aimed at a corner of a mirror. For this work, the upper frequency bound was set to 500 Hz with a resolutions of 1/4 Hz, requiring a sampling length of at least 4 seconds. To improve the quality of the results and measure coherence, while keeping test times reasonable, no more than 15 averages were used. For ambient excitation, sample sets were overlapped 50% for averaging, requiring 32 seconds per location. Testing 61 locations per mirror (366 locations total) took 3 1/4 hours for ambient. If distinct samples were used, such as with impact hammer excitation, testing would have required 15 hours.

During the test, regular activities were conducting outside the dark tent. Restricting all activity during testing was not feasible or desirable (since adaptive optics tests would be conducted during typical activity). As a result, the

ambient excitation power spectrum could be expected to change throughout the course of the test. Locations were tested without an obviously ordered sequence, so changes in disturbances would not necessary be organized spatially. Results showed that despite the less than ideal disturbances, clear results can be seen.

Follow-on laser vibrometry tests were conducted recently in 2013. These test focused on high frequency modes (100 to 600 Hz) in which finite element modeling predicted significant out-of-plane displacements of the mirror segments. To ensure strong coherence, a compact proof mass actuator (PMA) shaker was installed on mirror segments supports as the excitation source. The shaker replaced a tuned mass damper (TMD) previously installed on the system to target system fundamental frequencies below 30 Hz. The shaker was of similar size and weight of the replaced TMD. Up to 61 scan points along the mirror surfaces were scanned in order to obtain high resolution mode shapes of the mirror segment modes. Additionally, impact hammer tests were conducted, with input strikes at the mirror to support joints and up to 31 scan points on the mirror surface. During all follow-on tests, the data was processed using 5 averages and no overlapping. Scan times ranged from 10 to 20 minutes for each mirror segment, with data collected on 3 segments.

C. Vibration Measurements

Bending modes of the mirrors were observed with measurements taken near the triangular isogrid intersections. Three groups of modes were observed: saddle bending from 150 Hz to 170 Hz (Figure 10), drum modes from 240 Hz to 260 Hz (Figure 11) and a trefoil at 440 Hz (Figure 12). The amplitudes of vibration were able to be measured from 1.5 to 1.0 nm. Results show that despite measuring directly on the reflective surface and only using ambient excitation, the magnitude of high frequency vibrations can be measured. The range of frequencies (~ 20 Hz) also indicates small differences in symmetry despite identical segments designs.

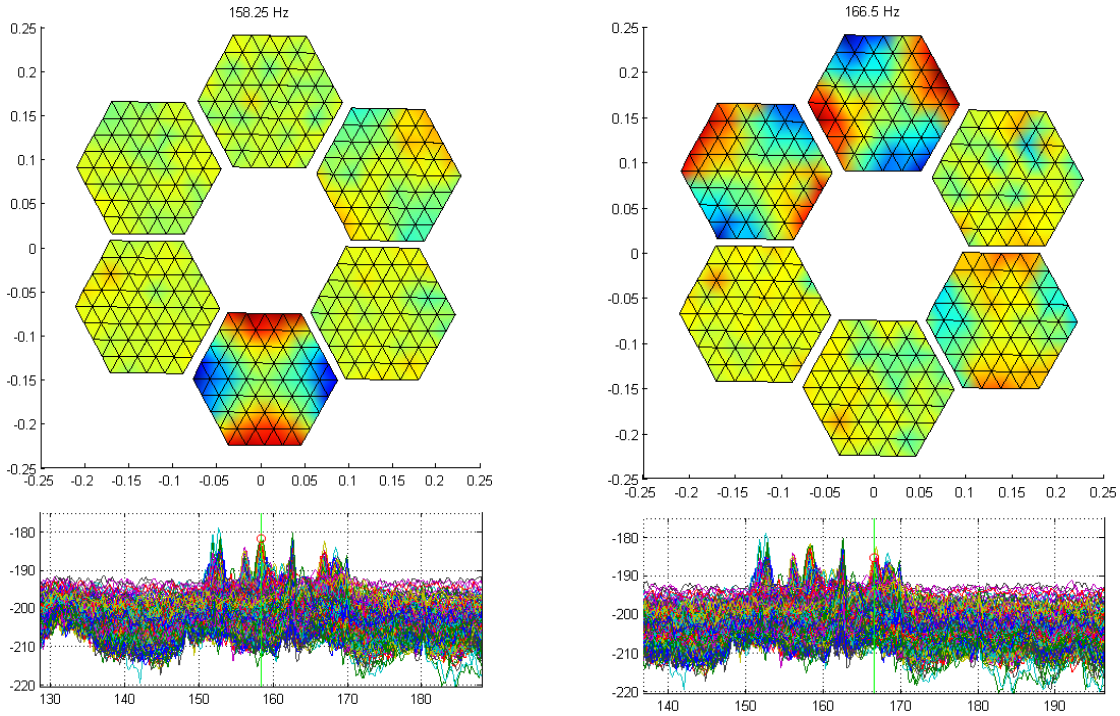

Figure 10. Saddle modes observed from 150 Hz to 170 Hz on all but one of the mirror.

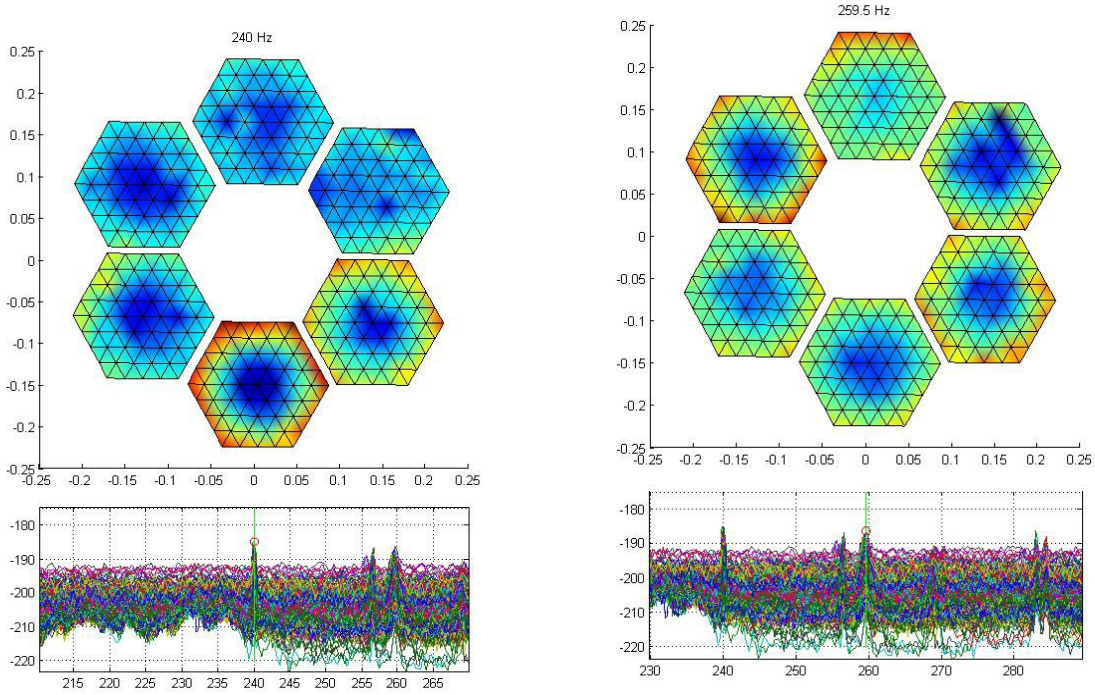

(a) (b)

Figure 11. Drum modes observed from 240 Hz to 260 Hz on all mirrors.

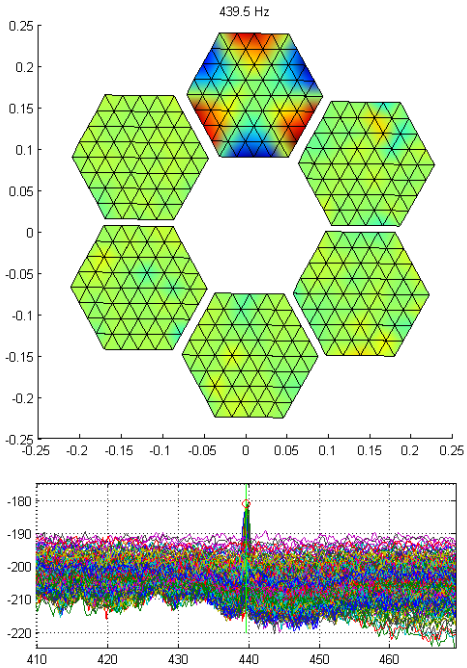

Figure 12. Trefoil mode observed at 440 Hz on a single mirror.

IV. Results

A. RO-mirror Static Comparison

Results of the RO- mirror model were very similar to the high fidelity model as desired. For qualitative comparison, the displacements for the load are given in Table 1. The RO-mirror model had 3.6% more displacements with differences in the direction being negligible. The displacement across the mirror is also qualitatively checked for similarity. Figure 13 shows the displacement contours of each model with results separated by the three orthogonal directions and the total displacement. The left edges are clamped with the load applied to the right vertex.

Table 1. Static Displacements

Model	Δ X	Δ Y	Δ Z
High Fidelity	0.1702	-0.01481	-0.8549
Reduced-Order	0.1763	-0.01547	-0.8858

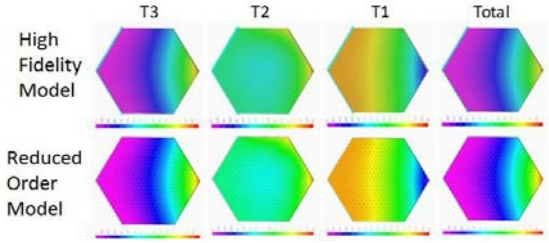

Figure 13. Displacements across the mirror for both models qualitatively agree.

B. RO-mirror Dynamic Comparison

With the initial mass properties, all the mode shapes agreed qualitatively with the high fidelity model. The density was adjusted to match the first frequency. A comparison of frequencies between the models is shown in Figure 14. The RO-mirror model under predicted the frequencies of higher modes by approximately 12%. The three modes described in section III.C, saddle, drum and trefoil, were matched to modes 1 and 2, mode 3 and mode 7, as shown in Figure 15, Figure 16, and Figure 17.

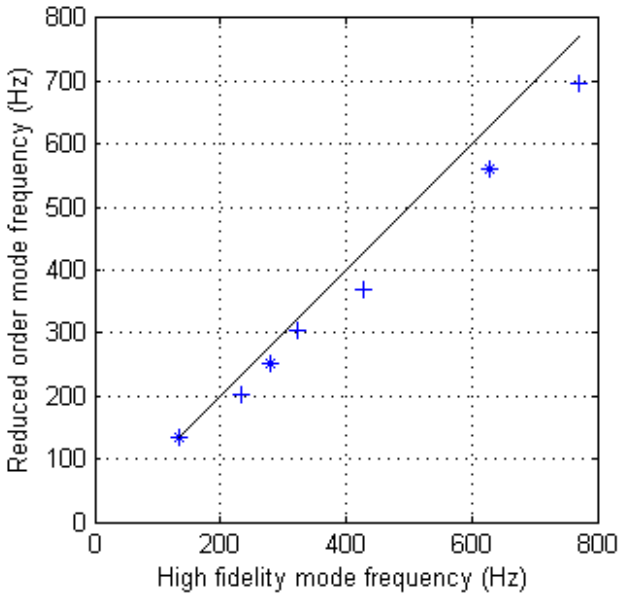

Figure 14. RO-mirror model under predicts higher frequencies.
(indicates 2 modes)*

Mode	RO-Mirror	Experimental	Hifi-Mirror
Saddle Mode			
2	134.11 Hz	150 - 170 Hz (all but 1 mirror)	134.08 Hz
			
	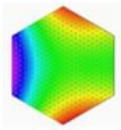		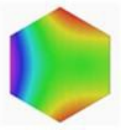

Figure 15. Saddle mode present in both models and in the experimental data.

Mode	RO-Mirror	Experimental	Hifi-Mirror
Drum Mode			
3	201.63 Hz	240 – 260 Hz (all mirrors)	232.32 Hz
	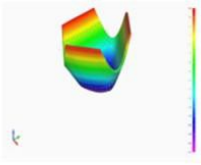		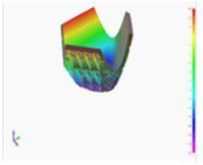
	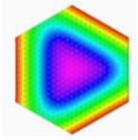	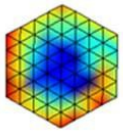	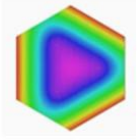

Figure 16. Drum mode present in both models and in the experimental data.

Mode	RO-Mirror	Experimental	Hifi-Mirror
Trefoil Mode			
7	368.76 Hz	439.5 Hz (single mirror)	429.20 Hz
	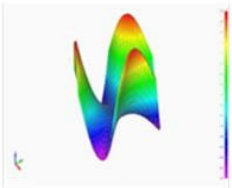		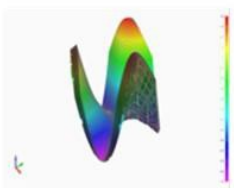
	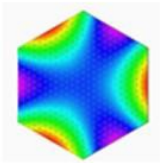	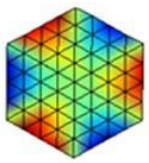	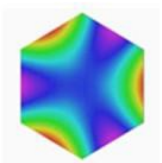

Figure 17. The trefoil mode is present in both models and in the experimental data.

C. Computational Comparison

Using the same computers, the high fidelity mirror required 44.9 seconds to process results, while the RO-mirror model only required 4.9 seconds. This represents an 89.1% reduction in the processing time required to analyze a simple load case on a mirror.

Lastly, the six RO-mirror segments were integrated into the residual partition of the substructured FEM. Table 2 presents a detailed comparison of model sizes, required simulation run times, and eigen analysis results prior to conducting tuning. Comparisons between the original HiFi-FEM, a reduced-order model with the RO-mirror segments (RO-FEM), the HiFi-FEM partitioned with superelements, and ROSE-FEM are shown. All comparison simulations were performed using MSC.Nastran on a Linux cluster node with 16 processors, 64 GB RAM, clocked on average over 400%. For the superelement partitioned simulations, SEID runs are sunk costs required only once, with follow-on tuning iterations on requiring only residual runs.

Table 2. FEM Simulation Comparisons (*SEIDs: superelement partitions require only 1 run)

	HiFi-FEM	**RO-FEM**	**HiFi-FEM with Superelements**	**ROSE-FEM**
dof:	2.63 M	1.38 M	residual: 1.49 M	residual: 0.24 M
nodes:	595 K	352 K	residual: 298 K	residual: 55 K
elements:	627 K	360 K	residual: 320 K	residual: 54 K
Simulation run time: (1st 10 modes)	2:17:55	not available	SEID1: 07:25:38 SEID2: 14:29:09 SEID3: 05:42:31 SEID4: 00:08:22 **residual:** 00:31:37	*SEIDs **residual:** 00:16:54
Required file memory (GB): (1st 10 modes)	160	76	SEID1: 15 SEID2: 31 SEID3: 8 SEID4: 8 **residual:** 31	*SEIDs **residual:** 4

As shown in Table 2, the combination of both superelement partitioning and isogrid equivalency model reduction methodologies yields substantial reduction in model size and efficiency. While a Linux cluster with unlimited virtual file memory was used to simulate all comparison runs, the superelement partitioned models have the advantage of requiring no more than 31 GB of temporary storage space. Because of this, simulations could be performed on a standalone desktop computer with limited storage capacity.

V. Conclusions and Future Work

This work presents a method for reducing model complexity so that model tuning and future analysis can be done with shorter processing times and is tractable for a desktop computer. Isogrid with equivalent plates are used based on the Isogrid Design Handbook.[14] Results show that the equivalent plates are similar to the high fidelity model, but show slightly less stiffness. Vibration data has been used for preliminary validation of the model.

Future work will address tuning of the model. Tuning to the measured data cannot be done directly on the RO-mirror model because the boundary conditions are different, and they directly impact the vibration frequency. With the RO-mirror incorporated, tuning the reduced-order superlement model to the high fidelity model will be done in terms of the material property design variables. The range of frequencies observed in the measured data can be used to estimate model uncertainty which is influenced by unmodeled items such as wiring harnesses, etc.

Acknowledgments

The authors would like to thank the Naval Postgraduate School for access to the telescope and hosting during testing. Adam Yingling of the Naval Postgraduate School provided invaluable assistance with his familiarity with the telescope. John Hamilton assisted Dr. Yingling mounting retro-reflective markers and John Bagnasco provided a CAD file which accelerated testing alignment. Albert Jordan provided direct assistance in vibration testing regarding setup of excitation sources.

References

[1] Beckers, J. M., "Adaptive Optics for Astronomy: Principles, Performance, and Applications," Annual review of astronomy and astrophysics , Vol. 31, Sep 1993, pp. 13–62, DOI: 10.1146/annurev.aa.31.090193.000305.

[2] Platt, B. C. and Shack, R., "History and principles of Shack-Hartmann wavefront sensing," Journal of Refractive Surgery , Vol. 17, No. 5, Sep-Oct 2001, pp. S573–7.

[3] Ellerbroek, B. L., Loan, C. V., Pitsianis, N. P., and Plemmons, R. J., "Optimizing closed-loop adaptive-optics performance with use of multiple control bandwidths," Journal of the Optical Society of America A, Vol. 11, No. 11, Nov 1994, pp. 2871–2886, DOI:10.1364/JOSAA.11.002871.

[4] Redding, D. C., Basinger, S. A., Lowman, A. E., Kissil, A., Bely, P. Y., Burg, R., Lyon, R. G., Mosier, G. E., Femiano, M., Wilson, M. E., Schunk, R. G., Craig, L. D., Jacobson, D. N., Rakoczy, J. M., and Hadaway, J. B., "Wavefront sensing and control for a Next-Generation Space Telescope," Space Telescopes and Instruments V , Vol. Proc. of SPIE 3356, Aug 1998, pp. 285, DOI: 10.1117/12.324494.

[5] Wasfy, T. M. and Noor, A. K., "Multibody dynamic simulation of the next generation space telescope using finite elements and fuzzy sets," Computer Methods in Applied Mechanics and Engineering , Vol. 190, No. 57, 2000, pp. 803
– 824, DOI: 10.1016/S0045-7825(99)00445-4.

[6] Chen, F.-L., Zhang, J.-X., Wu, X.-X., and Fan, L., "Supporting structure of 620 mm thin primary mirror and its active surface correction," Optics and Precision Engineering , Vol. 19, No. 5, May 2011, pp. 1022–1029.

[7] Honneger, B., "NPS New Home for Giant Segmented-Mirror Space Telescope," Press Release, Naval Postgraduate School, Monterey, California, Jan 2010.

[8] Burtz, D. C., Fine Surface Control of Flexible Space Mirrors Using Adaptive Optics and Robust Control , Ph.D. thesis, Naval Postgraduate School, Monterey, California, Mar 2009.

[9] Axtell, T. W., Segmented Mirror Telescope Model and Simulation , Master's thesis, Naval Postgraduate School, Monterey, California, Jun 2011.

[10] Jennings, A. L. and Cobb, R., "Ambient Vibration Testing of a Segmented Mirror Telescope," 54th AIAA/ASME/ASCE/AHS/ASC Structures, Structural Dynamics, and Materials Conference , Space and Launch Vehicle Structural Dynamics, Boston, MA, Apr 2013, pp. 1–15, DOI: 10.2514/6.2013-1884.

[11] Qu, Zu-Qing. Model Order Reduction Techniques: With Applications in Finite Element Analysis. London: Springer, 2004.

[12] Lavin, J., Buckling of Isogrid Plates , Master's thesis, Rensselaer Polytechnic Institute, Hartford, CT, Jun 2010.

[13] Blunck, K., Coon, T. E., Swenson, E., Black, J., and Cobb, R., "Space Telescope Structural Design Analysis for the Chromotomographic Hyperspectral Imaging Experiment," 54th AIAA/ASME/ASCE/AHS/ASC Structures, Structural Dynamics, and Materials Conference , Space Structures, Boston, Apr 2013, pp. 1–10.

[14] Meyer, R. R., Harwood, O., and Orlando, J., “Isogrid Design Handbook,” Tech. Rep. MDC G4295A/NASA CR-124075, McDonnell Douglas Astronautics Company, Huntington Beach, CA, Feb 1973, For NASA Marshall Space Flight Center, contract NAS 828619.

[15]Yingling, A. J., Integrated Structures, Optics, and Controls of the Segmented Mirror Telescope , Ph.D. thesis, Naval Postgraduate School, Monterey, California, Sep 2012.

Appendix C. FEM Response Surface Characterization with FCD

FCD design, with corresponding eigenanalysis run times and results. $J_{\#}$ represents the objective function specific for each segment under consideration. Tuning was completed using E values predicted to minimize the objective function ($J \approx 0$).

	Coded Units										
	X 1	X 2	X 3	X 4	Run Time	Seg 4 1st Freq	J_4	Seg 5 1st Freq	J_5	Seg 6 1st Freq	J_6
Full Factorial	-1	-1	-1	-1	5:40	157.570	6.6	155.218	-3.8	157.611	-3.4
	1	-1	-1	-1	4:50	178.451	27.5	161.792	2.8	177.050	16.0
	-1	1	-1	-1	5:05	165.568	14.6	159.440	0.4	165.568	4.6
	1	1	-1	-1	4:56	185.815	34.8	162.255	3.3	180.073	19.1
	-1	-1	1	-1	4:40	173.729	22.7	161.284	2.3	173.208	12.2
	1	-1	1	-1	4:56	193.475	42.5	193.992	35.0	193.499	32.5
	-1	1	1	-1	12:06	181.361	30.4	161.988	3.0	178.707	17.7
	1	1	1	-1	10:56	200.419	49.4	201.073	42.1	200.419	39.4
	-1	-1	-1	1	11:46	168.883	17.9	160.344	1.3	168.689	7.7
	1	-1	-1	1	11:47	188.849	37.8	189.328	30.3	188.871	27.9
	-1	1	-1	1	11:57	177.794	26.8	161.614	2.6	176.608	15.6
	1	1	-1	1	4:30	196.883	45.9	197.501	38.5	196.883	35.9
	-1	-1	1	1	4:20	184.129	33.1	179.705	20.7	179.705	18.7
	1	-1	1	1	4:21	203.106	52.1	203.894	44.9	203.106	42.1
	-1	1	1	1	11:20	192.567	41.6	193.100	34.1	192.589	31.6
	1	1	1	1	11:06	210.636	59.6	211.715	52.7	210.625	49.6
Axial	-1	0	0	0	4:35	157.571	6.6	155.219	-3.8	157.611	-3.4
	1	0	0	0	4:16	178.452	27.5	161.792	2.8	177.050	16.1
	0	-1	0	0	4:31	157.571	6.6	155.219	-3.8	157.611	-3.4
	0	1	0	0	6:45	165.707	14.7	159.440	0.4	165.569	4.6
	0	0	-1	0	12:47	157.570	6.6	155.219	-3.8	157.611	-3.4
	0	0	1	0	16:02	173.729	22.7	161.284	2.3	173.209	12.2
	0	0	0	-1	12:17	157.570	6.6	155.219	-3.8	157.611	-3.4
	0	0	0	1	11:46	168.884	17.9	160.344	1.3	168.690	7.7
cp	0	0	0	0	4:25	157.572	6.6	155.220	-3.8	157.619	-3.4

*cp – center point

References

Baiocchi, D., & Stahl, H. P. (2010). Enabling Future Space Telescopes: Mirror Technology Review and Development Roadmap. *The Astronomy and Astrophysics Decadal Survey, Technology Development Papers (NASA), no. 23*.

Caltech, University of California. (2014, Feb 19). *About TMT*. Retrieved from Thirty Meter Telescope: http://www.tmt.org/about-tmt

Cobb, R. G., & Sullivan, J. M. (1999). Vibration isolation and suppression system for precision payloads in space. *Smart Materials and Structures*, 798-811.

Genberg, V., Bisson, G., Michels, G., & Doyle, K. (2006). External Superelements in MSC Nastran, a Super Tool for Segmented Optics. *MSC.Software VPD Conference.* Huntington Beach, CA.

Gibson, L., & Ashby, M. (1988). *Cellular Solids.* New York: Pergamon Press.

Hecht, E. (2002). *Optics, 4th Ed.* San Francisco: Addison Wesley.

Jennings, A. L., & Cobb, R. G. (2013). Ambient Vibration Testing of a Segmented Mirror Telescope. American Institute of Aeronautics and Astronautics.

Lane, S. A., & Lacy, S. L. (2008). Active Vibration Constrol of a Deployable Optical Telescope. *Journal of Spacecraft and Rockets*, 568.

Marwala, T. (2010). *Finite-element-model Updating Using Computational Intelligence Techniques.* London: Springer.

McDonnell Douglas Astronautics Company. (1973). *Isogrid Design Handbook.* NASA Contractor Report, Huntington Beach, CA.

Meza, L., Tung, F., Anandakrishnan, S., Spector, V., & Hyde, T. (2005). Line of Sight Stabilization of James Webb Space Telescope. *American Astronautical Society Guidance and Control Conference* (pp. 1-15). Breckenridge, CO: AAS Publications Office.

Myers, R. H., Montgomery, D. C., & Anderson-Cook, C. M. (2009). *Response Surface Methodology, 3rd ed.* Hoboken, NJ: John Wiley & Sons, Inc.

NASA. (2014, February 12). *James Webb Space Telescope*. Retrieved from Wikipedia: http://en.wikipedia.org/wiki/James_Webb_Space_Telescope

O'Keefe, K. (2011). Dynamic Modeling Methodology. *International Conference on Space Optical Systems and Applications* (pp. 157-163). IEEE.

Qu, Z.-Q. (2004). *Model Order Reduction Techniques: With Applications in Finite Element Analysis.* London: Springer.

Schwartz, E. (2013). AMD Active Hybrid Mirror Segment Development. *NPS Workshop on Applications of Adaptive Optics to Imaging Satellites.* Monterey, CA.

Yingling, A. J. (2012). *Integrated Structures Optics and Controls of the Segmented Mirror.* Monterey, CA: Naval Postgraduate School.

Vita

Captain Luke C. Dras graduated from Buena Vista High School in Buena Vista, Colorado. He is a 2006 graduate of Embry-Riddle Aeronautical University in Prescott, Arizona with an undergraduate degree in Aerospace Engineering.

Captain Dras previously served as the AETC lead T-6A and T-1A operational test engineer, overseeing multi-disciplined teams in the planning, execution, analysis, and reporting of effectiveness and suitability of AETC's flying training systems. In addition, he led AETC's technology innovation test team performing assessments of Advanced Learning Technology Demonstrations aimed at bringing 21st century technology into the Air Force classroom.

Prior to entering the Graduate School of Engineering and Management, Air Force Institute of Technology, Captain Dras served as the Assistant Director of Operations, AFOTEC Det 5, where he advised detachment leadership on operational test and evaluation activities for 31 aircraft systems with acquisition costs of over 102 billion dollars. His portfolio included operational assessments and evaluations of bomber, mobility, C2ISR, special operations, and training aircraft systems.

Upon graduation, he will be assigned to the AFRL Aerospace Systems Directorate at Edwards AFB, California.

REPORT DOCUMENTATION PAGE			Form Approved OMB No. 0704-0188

1. REPORT DATE *(DD-MM-YYYY)*	2. REPORT TYPE	3. DATES COVERED *(From - To)*
27-03-2014	Master's Thesis	September 2012 - March 2014

4. TITLE AND SUBTITLE
Model Uncertainty and Test of a Segmented Mirror Telescope

5a. CONTRACT NUMBER

5b. GRANT NUMBER

5c. PROGRAM ELEMENT NUMBER

6. AUTHOR(S)
Luke C. Dras, Captain, USAF

5d. PROJECT NUMBER
JON 14Y153

5e. TASK NUMBER

5f. WORK UNIT NUMBER

7. PERFORMING ORGANIZATION NAME(S) AND ADDRESS(ES)
Air Force Institute of Technology
Graduate School of Engineering and Management (AFIT/EN)
2950 Hobson Way
Wright-Patterson AFB OH 45433-7765

8. PERFORMING ORGANIZATION REPORT NUMBER
AFIT-ENY-14-M-18

9. SPONSORING/MONITORING AGENCY NAME(S) AND ADDRESS(ES)
Naval Postgraduate School
699 Dyer Road
Monterey CA 93943
Brij N. Agrawal, Ph.D., agrawal@nps.edu

10. SPONSOR/MONITOR'S ACRONYM(S)
NPS

11. SPONSOR/MONITOR'S REPORT NUMBER(S)

12. DISTRIBUTION/AVAILABILITY STATEMENT
Distribution Statement A. Approved for Public Release; Distribution Unlimited

13. SUPPLEMENTARY NOTES
This material is declared a work of the U.S. Government and is not subject to copyright protection in the United States.

14. ABSTRACT

Today's monolithic mirror technology has reached a barrier, particularly for space-based telescopes. These large diameter, dense mirrors allow stable high- resolution imaging but are incompatible with space launch. Segmented mirror telescopes, optimized to be lightweight, are configurable for compact stowage. High-fidelity finite element models are commonly used to economically predict how the optics will perform under different environmental conditions. The research detailed herein integrates superelement partitioning and complexity simplifying techniques, resulting in a 92% size reduction of a nodally dense (>1x106 degrees of freedom) model to allow efficient tuning and validation. Measured vibration data of a segmented mirror telescope was collected to allow system characterization and preliminary tuning. A single frequency comparison tuning iteration decreased the model's error in predicting system dynamics, up to 500 Hz, by 4% on average. The methodologies presented, applied to similar models with complex isogrid structures, would allow efficient model validation using standard equipped US Air Force desktop computers.

15. SUBJECT TERMS
segmented mirror telescope, finite element analysis, modeling, modal testing, vibration damping and control

16. SECURITY CLASSIFICATION OF:			17. LIMITATION OF ABSTRACT	18. NUMBER OF PAGES	19a. NAME OF RESPONSIBLE PERSON
a. REPORT	b. ABSTRACT	c. THIS PAGE			Richard G. Cobb, Ph.D., AFIT/ENY
U	U	U	UU	91	19b. TELEPHONE NUMBER *(Include area code)* (937) 255-3636 x4559 richard.cobb@afit.edu

Standard Form 298 (Rev. 8/98)
Prescribed by ANSI Std. Z39.18